From THE DEPARTMENT OF CLINICAL SCIENCE,
INTERVENTION AND TECHNOLOGY
Karolinska Institutet, Stockholm, Sweden

OPTIMIZING COMPUTED TOMOGRAPHY: QUALITY ASSURANCE, RADIATION DOSE AND CONTRAST MEDIA

Patrik Nowik

Stockholm 2020

All previously published papers were reproduced with permission from the publisher.
Published by Karolinska Institutet.
Printed by E-Print AB 2020
© Patrik Nowik, 2020
ISBN 978-91-7831-659-5

OPTIMIZING COMPUTED TOMOGRAPHY: QUALITY ASSURANCE, RADIATION DOSE AND CONTRAST MEDIA
THESIS FOR DOCTORAL DEGREE (Ph.D.)

By

Patrik Nowik

Principal Supervisor:
Docent Torkel B Brismar
Karolinska Institutet
Department of Clinical Science, Intervention and Technology
Division of Radiology

Co-supervisor:
Doctor Gavin Poludniowski
Karolinska Institutet
Department of Oncology-Pathology
Division of Oncology

Opponent:
Professor Mika Kortesniemi
University of Helsinki
Department of Diagnostics and Therapeutics

Examination Board:
Docent Anne Thilander Klang
Göteborgs Universitet
Department of Radiation Physics
Institute of Clinical Sciences

Professor Håkan Geijer
Örebro Universitet
School of Medical Sciences

Professor Michael Sandborg
Linköpings Universitet
Department of Medical and Health Sciences
Division of Radiological Sciences

ABSTRACT

Computed tomography (CT) is an important modality in radiology; it enables imaging of the inside of patients without superimposed anatomy. The radiation dose and quality of a CT image are highly dependent on the CT scanner, the scan settings and, if applicable, the timing and dosage of the intravenous contrast media (CM). The aim of this Thesis was to develop tools and insights that help maximize the value of examinations for patients undergoing CT and to reduce its cost in terms of radiation and CM dose. The Thesis consists of five studies.

The first paper was on quality control (QC) of CT, which is the foundation for a radiology clinic: it provides trust that the equipment functions as expected. A new method of performing routine QCs was proposed where the concept of key performance indicators (KPI) was introduced, together with a semi-automatic process allowing for daily QCs. During the time of the study, multiple deviations were discovered that would have been difficult to detect using traditional QCs. Performing QCs more frequently facilitates more extensive trend analysis.

The second paper was on automatic tube current modulation (ATCM). A phantom and a method for the characterization of ATCM were developed. These allowed for a characterization of CT scanners from the four main CT vendors in Sweden, summarized in four extensive tables showing how the ATCM responds to changes in scan parameters. More specifically, the tables present how changes in scan settings of the localizer radiograph (LR), scan settings of the acquisition, reconstruction parameters and patient miscentering affect the ATCM.

The third paper was on radiation dose estimation uncertainties coupled to the patient table. In most commercial radiation dose estimation software packages for CT, the patient table is not included. That effect was previously unknown but could be shown using Monte Carlo (MC) calculations of CT scans performed with and without the patient table. It was shown that by not including the effect from the patient table in radiation dose estimations, the radiation doses are overestimated by 5% to 23%, depending on the scan mode.

The fourth paper evaluated whether the standard LR can be replaced by a low-dose spiral scan, a so-called synthetic LR (SLR). Such an SLR can potentially improve ATCM, CM dosage and CT planning. Radiation doses were estimated using MC, the image quality was compared in a prospective study of ten patients and the impact of miscentering was investigated with a phantom measurement of water equivalent diameters. It was shown that the radiation doses and the image quality of SLR and LRs were similar. Estimated water equivalent diameters were more consistent when calculated from the low-dose spiral scan compared to the LRs. It was concluded that it is feasible to replace the traditional LR with an SLR for CT scan planning.

The fifth paper was a continued investigation of the low-dose spiral scan, but with focus on intravenous CM dosage planning. Altogether, 238 patients who had undergone PET/CT and

for whom body metrics (height and weight) had been acquired were retrospectively analyzed, the CT number enhancement of the liver was measured, and body volumes of muscle and fat were calculated using the attenuation correction CT (low-dose spiral scan). Multiple linear regressions showed that for CM dose planning, the body volumes of muscle and fat are better to use than body weight. However, the adjusted R^2 values of all the investigated models were low, indicating that responses to CM dosage are complex and require more research.

In this PhD Thesis, tools and insights were developed to improve the imaging stability of the CT scan by developing semi-automatic QC protocols and techniques to better estimate patient size and shape potentially reducing variation in image quality, radiation dose and CM enhancement among patients.

LIST OF SCIENTIFIC PAPERS

I. **Nowik P**, Bujila R, Poludniowski G, Fransson A, *Quality control of CT systems by automated monitoring of key performance indicators: a two-year study*, 2015, Journal of Applied Clinical Medical Physics 16 (4)

II. Merzan D, **Nowik P**, Poludniowski G, Bujila R, *Evaluating the impact of scan settings on automatic tube current modulation in CT using a novel phantom*, 2017, The British journal of radiology 90 (1069)

III. **Nowik P**, Bujila R, Kull L, Andersson J, Poludniowski G, *The dosimetric impact of including the patient table in CT dose estimates*, 2017, Physics in Medicine & Biology 62 (23)

IV. **Nowik P**, Poludniowski G, Svensson A, Bujila R, Morsbach F, Brismar T, S, *The synthetic localizer radiograph – A new CT scan planning method*, 2019, Physica Medica 61

V. **Nowik P**, Poludniowski G, Svensson A, Thor D, Bujila R, Brismar T, *Intravenous contrast media dosage for CT scanning: are muscle and fat volumes segmented from a low-dose CT pre-scan better predictors of enhancement than body weight?*, 2019, Manuscript

CONTENTS

LIST OF ABBREVIATIONS

2D	Two dimensions
3D	Three dimensions
AAPM	American Association of Physicists in Medicine
ACCT	Attenuation correction CT
AI	Artificial intelligence
AIC_C	The second-order Akaike information criterion
ATCM	Automatic tube current modulation
BH	Body height
BP	Back-projection
BW	Body weight
CI	Confidence interval
CM	Contrast media
CNR	Contrast to noise ratio
CT	Computed Tomography
CTDI	CT dose index
DLR	Deep learning reconstruction
DLP	Dose length product
E	Effective dose
EMI	Electric and Musical Industries
FBP	Filtered back-projection
HU	Hounsfield unit
ICRP	International Commission on Radiological Protection
IEC	International Electrotechnical Commission
IR	Iterative reconstruction
KAP	Kerma area product
KPI	Key performance indicator
LBM	Lean body mass
LR	Localizer radiograph
LSF	Line-spread function
MC	Monte Carlo

MTF	Modulation transfer function
NPS	Noise power spectrum
NRMSE	Normalized root mean squared error
NRPB	National Radiological Protection Board (in UK)
PET	Positron emission tomography
PMMA	Polymethyl methacrylate
ROI	Region of interest
QA	Quality assurance
QAC	Quality assurance committee
QC	Quality control
SLR	Synthetic localizer radiograph
SSM	The Swedish Radiation Safety Authority (Strålsäkerhetsmyndigheten)
SSP	Slice sensitivity profile
V_{FAT}	Body volume of fat
V_{MUSCLE}	Body volume of muscle
WED	Water equivalent diameter
WL	Window level
WW	Window width

1 INTRODUCTION

The first X-ray radiograph was obtained in 1895 by Wilhelm Conrad Röntgen [1] starting a revolution in healthcare [2]. It gave medical doctors the tool to see pathology inside the body without performing surgery. Typically, a radiograph is performed with an X-ray tube on one side of the patient and a detector on the other side. For a short duration, the X-ray tube emits X-rays, the majority of which interact in the patient. Different tissues attenuate the X-rays to different extent, resulting in variations in the number of photons passing through to the detector. Even though the resulting image of the anatomy is only in two dimensions (2D) it is extremely helpful.

In 1917, the mathematical foundation to CT was developed by Johann Radon [3]. However, it was not until after the development of computers when a CT scanner could be constructed in the early 1970s [4]. Using CT, anatomy could now be visualized without being superimposed, yielding rapid and non-invasive investigation of the anatomy of patients, revealing previously obscured diagnostic information. In Figure 1.1, radiographs and CT images from abdomen and lung examinations are demonstrated, where structures can clearly be seen in the CT images.

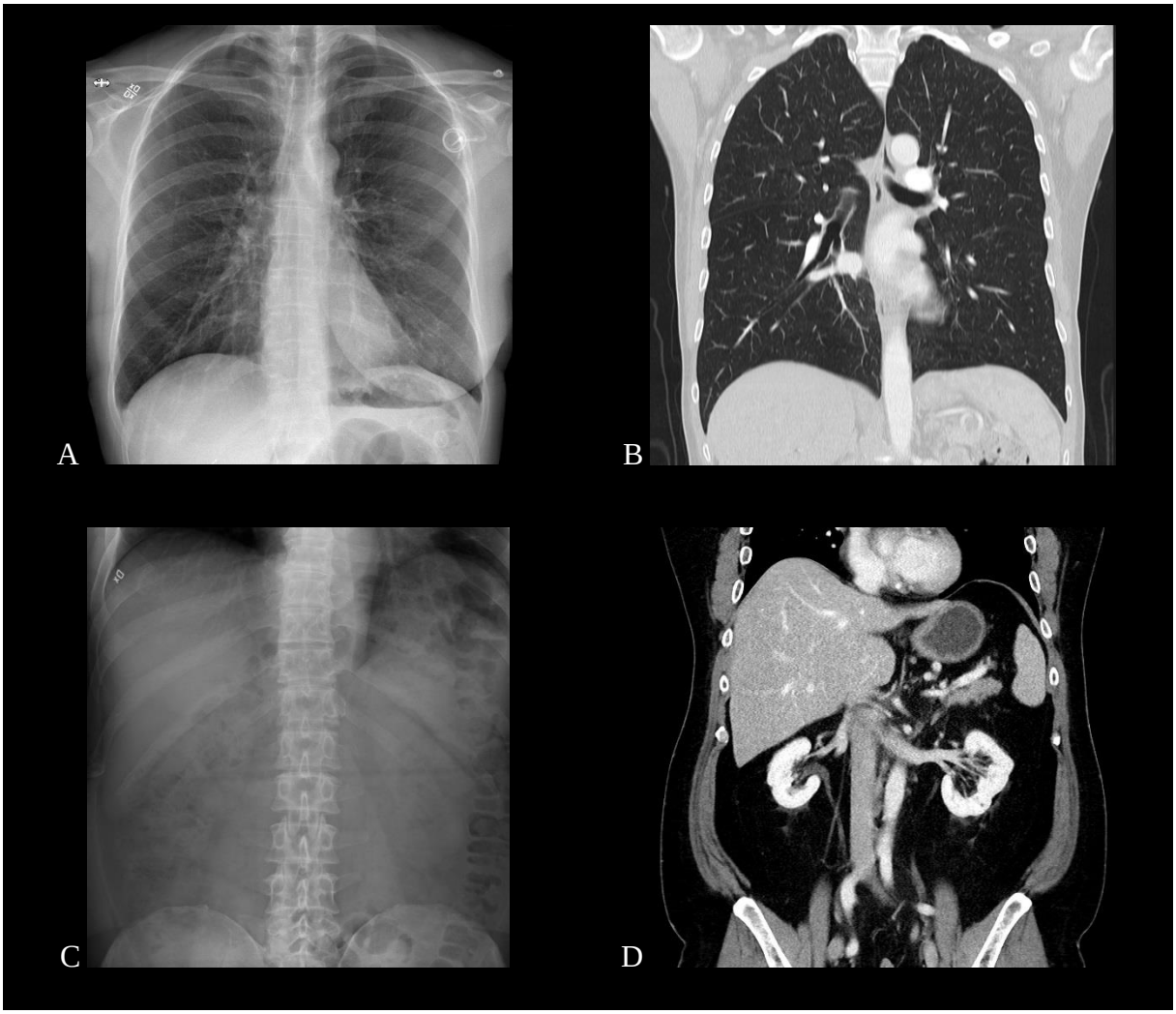

Figure 1.1. Radiographs of the lung (**A**) and abdomen (**C**) and CT images of the thorax (**B**) and abdomen (**D**), of two patients from **Paper V**.

Since then, the technical development has been rapid [5]. Further, CT can now be combined with other modalities such as positron emission tomography (PET, together called PET/CT) for fusion of anatomical and functional data (hybrid imaging) [6].

The modality CT is a large contributor to the collective radiation dose. For example, during year 2014, some 8% of the medical examinations in Germany were CT examinations, while the collective dose to the population from CT examinations was 64% [7]. To reduce the high collective radiation dose from CT it is of importance to improve its use.

One of the main tasks of a medical physicist working clinically in the field of X-ray diagnostics is to maintain and supervise quality assurance (QA) programs of the X-ray equipment [8]. Via QA programs, it is ensured that all examinations are performed at the highest standard. As a part of a QA program, the quality control (QC) is a group of separate tests of the technical status of the equipment to ensure that it is running as intended. Historically, such QCs were performed annually on each X-ray equipment by the clinical medical physicists, taking up most of their time. Nowadays, the main role of a medical physicist at an X-ray physics department is changing, with more and more attention to CT optimization. In Sweden, optimization of CT is typically performed by a QA committee (QAC), consisting of a medical physicist, a radiologist and a CT technologist [9]. The main task of such a group is to handle questions and parameters regarding the quality of the CT scans: QA of the CT scanner, methodology of examinations and CT scan protocols. Optimization of CT is the process of improving a CT examination, typically a CT scan protocol, maximizing image quality while minimizing radiation dose to the patient. The main challenge in CT optimization is that image quality and radiation dose are correlated, forcing the QAC group to compromise. This is the reason for X-ray equipment to have multiple pre-programmed ways of acquiring images (called examination protocols). The medical physicist's primary role in the QAC group is to provide knowledge about all functions of the X-ray equipment and their effect on image quality and radiation dose. One specific function which medical physicists typically strive to understand is the automatic tube current modulation (ATCM). This is a function that adapts the dose from the X-ray tube to produce a uniform image quality throughout the examination. The ATCM algorithm is different between CT scanners and is, therefore, a good example of a function that medical physicists should understand well. Moreover, having an active QA program in radiology is mandatory by the Swedish Radiation Safety Authority (SSM, Strålsäkerhetsmyndigheten) [10].

1.1 AIM OF THE PROJECT

The aim of this PhD project was to develop tools and insights that help clinical medical physicists maximize the outcome of examinations for patients undergoing CT and minimize its costs. This corresponds to increasing the diagnostic certainty of the CT scan, reducing patient dose and making the process of CT scanning better and easier for both the patient and the CT technologist. Split into five studies, the specific aims were:

- to develop a QC method enabling more frequent CT QCs, without increasing staff workload (**Paper I**) [11],
- to develop a methodology to characterize the ATCM function, independent of CT scanner model, and to use it on CT scanners from different vendors at our institution (**Paper II**) [12],
- to examine how the patient table affects the estimation of CT dose (**Paper III**) [13],
- to create a synthetic localizer radiograph (SLR) from a low-dose 3D scan and to estimate its potential to replace the conventional localizer radiograph (LR) (**Paper IV**) [14],
- to investigate whether the low-dose 3D scan might be used to reduce the variation contrast media (CM) enhancement of the liver among patients (**Paper V**).

2 X-RAY COMPUTED TOMOGRAPHY

2.1 TECHNOLOGY

The first step towards producing a CT image is the creation of radiation, which is done in the X-ray tube. It is a vacuum tube which has a cathode and an anode, where the cathode emits electrons into the vacuum, hitting the anode. An applied voltage between the cathode and the anode (the tube voltage) accelerates the electrons and controls the energy of the resulting X-ray spectrum. The electrical current flowing between the cathode and the anode (the tube current) controls the number of photons generated. Around 1% of the energy results in emitted photons, and the other 99% turns into heat. Most photons are created through an interaction called bremsstrahlung, while some are created through characteristic radiation. Bremsstrahlung is the electromagnetic radiation (photons) that is created from the energy that electrons lose when deaccelerated by deflection in the electric field from the atomic nucleus in the anode material. Characteristic radiation is that of photons that are created with the energy from an electron transition in an excited atom. The excitation occurs when an electron in an inner shell of an atom of the anode material is hit by an incident electron or a bremsstrahlung photon with an energy exceeding the binding energy. This inner shell electron transits to a higher energy level and leaves a vacancy in its former shell. When an electron returns from the outer shell to the inner shell the characteristic radiation is emitted.

The X-rays emitted from the X-ray tube will then be affected by the objects (tissues) they pass before reaching the detector. The effect from the tissue can be described by three different principles, all relevant for the energy range in CT: Rayleigh scattering, Compton scattering and photoelectric effect. Rayleigh scattering occurs mainly at very low energies. An incident photon excites a whole atom, which radiates this extra energy in the form of a new photon with the same energy, but in a slightly different direction. In radiology, the main interaction process in soft tissues is Compton scattering. The incident photon hits an electron of an atom that then gets ejected from its shell. The incident photon does not use all its energy and gets scattered in another direction with less energy. The probability of Compton scattering is approximately proportional to the density of the material. The photoelectric effect is also important and occurs when an incident photon hits an electron of an atom that gets ejected from its shell. However, in this interaction, the photon transfers all its energy to the electron. For this to happen, the incident photon must have an energy equal to or slightly higher than the binding energy of the electron. The atom is left in an excited state. To stabilize the atom, an electron from an outer shell returns to the inner shell emitting characteristic radiation.

To produce a CT image, several projections around the object are needed. To optimize the amount of radiation passing through the body reaching the detector, a shaped filter (commonly also called bow-tie filter, Figure 2.1) is used. It filters the X-ray beam to balance the varying amount of projected tissue that the X-rays will pass through due to the elliptical

nature of the human body. The center of the patient needs most radiation due to greater thickness and denser material. The use of a shaped filter assumes a centered patient.

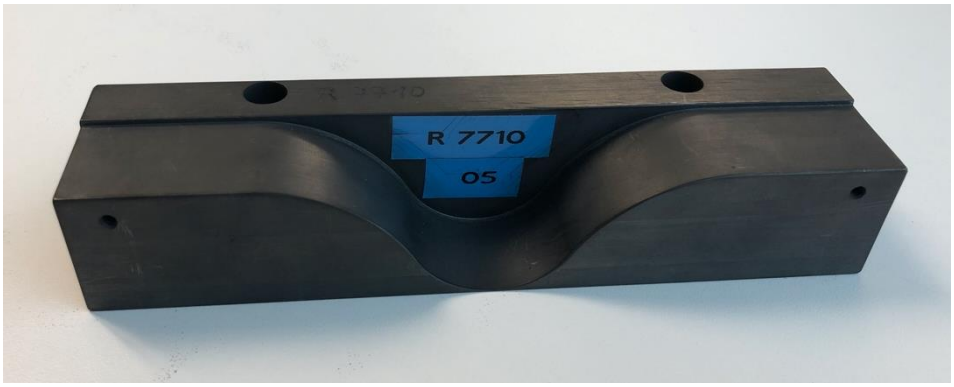

Figure 2.1. A CT shaped filter. Courtesy of Sebastian Faby (Siemens Healthcare, Forchheim, Germany).

The current generation of CT detectors is built in two layers, a scintillator and a photodiode. The scintillator transforms the photon into light, which is detected by the photodiode and transformed into an electric current. The detector signal is integrated, meaning that the energies of the individual photons are not resolved in the signal. This might change in the near future with the development of photon-counting detectors [15, 16]. The signal from a full detector row is used for each projection. To create a CT image, projections from at least a half rotation are needed (normally a full rotation is used).

The acquisition of projections around the body starts with detection of the intensity signal $I = I_0 \cdot e^{-\int_0^d \mu(x,y,z)\,ds}$, where I_0 is the intensity with the object removed. The linear attenuation of each material in the position (x,y,z) is $\mu(x,y,z)$, the thickness of the material is s and the length of the path is d. Further, the intensity is transformed to the total attenuation of the path (the line integral): $\ln\left(\frac{I}{I_0}\right) = -\int_0^d \mu(x,y,z)\,ds$. In Figure 2.2, a representation of three circular objects and calculated projections from two different angles are demonstrated.

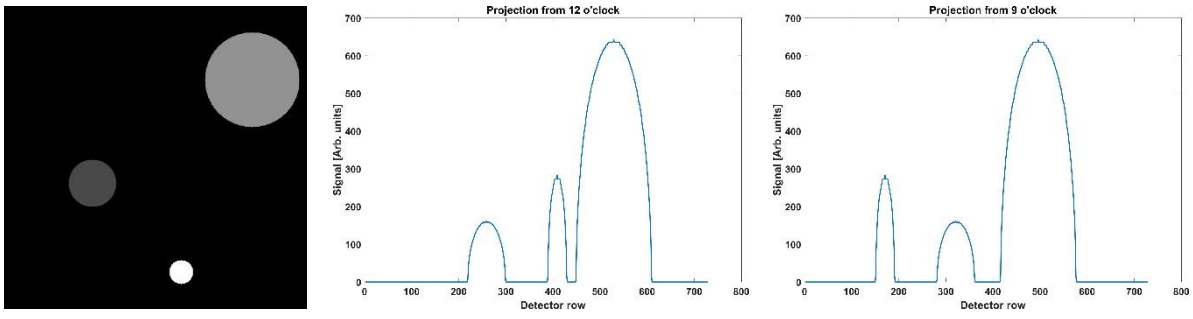

Figure 2.2. A representation of three circular objects (**left**) and how CT projections would look like with the X-ray tube stationary at 12 o'clock (**middle**) and 9 o'clock (**right**). Figures created using MATLAB (version r2019b, MathWorks Inc., Natick, MA).

The pixel values in a CT image correspond to the linear attenuation of the object, μ. To remove the dependence on energy from μ, the pixel values are represented as a relative

variation with respect to water as a reference material. The pixel values are called CT numbers and are defined using the quotient $1000 \cdot \frac{\mu_{\text{object}} - \mu_{\text{water}}}{\mu_{\text{water}}}$.

The unit of CT numbers is the Hounsfield unit (HU). From the CT number quotient, it can be derived that, ideally, the CT number of water has a value of 0 HU and that the CT number of air is -1000 HU. CT scanners are calibrated to ensure those CT numbers are within a certain tolerance. In practice, a small variation of CT numbers is expected. Since CT images are affected by noise, the CT number should always be measured as a mean pixel value in a region of interest (ROI). Typical CT numbers for fat, muscle and bone are -190 HU to -30 HU (fat), -30 HU to 200 HU (muscle) and >200 HU (bone) [17].

CT images are usually 12 bits per voxel, with CT numbers ranging between -1024 HU and 3072 HU. The human eye cannot distinguish among so many grayscales. Thus, the displayed range of CT images typically is mapped to include the CT numbers of interest. The range is called the window settings and consists of the window width (WW) and window level (WL). The WL specifies the center of the range and the WW specifies the range of CT numbers included. Figure 2.3 shows an axial image of a patient (from **Paper V**) with three different window settings.

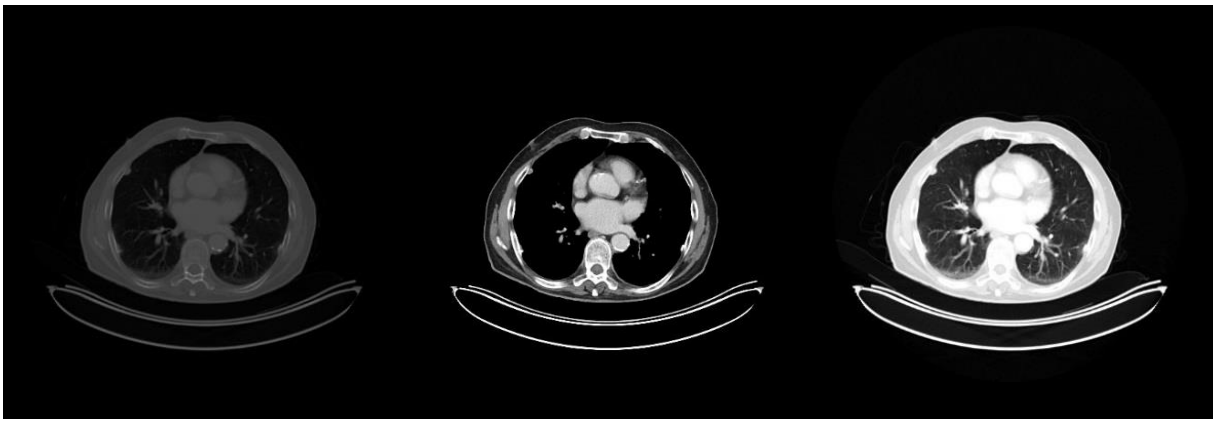

Figure 2.3. An axial image of the thorax (patient from **Paper V**) with three different levels of window settings: WL: 1000 WW: 4000 (**left**), WL: 50 WW: 400 (**middle**, typical settings for the abdomen) and WL: -600 WW: 1500 (**right**, typical settings for the chest).

In CT, scanning can be divided into three major scan modes: LR, axial scanning and spiral scanning. An LR is a radiographic planning image acquired with the X-ray tube and detector both stationary, where the X-ray tube is irradiating while the patient moves through the gantry opening to create a radiography-like image. Axial scanning is when the detector signal around the patient is collected with the patient stationary while the X-ray tube and detector rotate. Spiral scanning is when the X-ray tube and detector rotate continuously while the patient moves through the gantry opening. The patient table speed during the spiral scan is defined as the pitch p:

$$p = \frac{\Delta\tilde{d}}{N \cdot T}, \tag{2.1}$$

where $\Delta\tilde{d}$ is the patient table distance moved for each gantry rotation, T is the thickness of a detector row and N is the number of rows used in the acquisition ($N \cdot T$ is the collimation of the scan).

2.2 DOSIMETRY

The absorbed dose is quantified by measuring the deposited energy per unit of mass. The basic unit for radiation dose is gray (Gy), which is defined as J/kg. This, however, is not patient dose. For the latter, biological effects must be considered. Different types of radiation have different biological effects per absorbed dose, making it necessary to correct for radiation type. The absorbed dose corrected for biological effect is called the equivalent dose, with the unit sievert (Sv). Gamma rays (X-rays) have a weighting factor of 1, while the weighting factor can vary with up to 20 for alpha particles. However, Task Group 79 of the International Commission on Radiological Protection (ICRP) discusses whether the use of equivalent dose should be discontinued and instead endorse the use of absorbed dose. The radiation dose to the patient is calculated as the weighted sum of the equivalent dose in specified organs and it is called the effective dose (E). It is also measured in the unit Sv, but it is the weighted sum of the equivalent dose in specified organs. The weighting depends on the organ's radiation sensitivity. A widely used figure of radiation risk is a 5% increase in fatal cancer after a whole-body exposure of 1 Sv [18]. In Sweden, an average person is exposed to 2.4 mSv / year, of which 0.9 mSv correspond to the national mean dose from medical examinations [19].

The radiation dose distribution differs between radiography and CT. In radiography, the dose is decreasing in one dimension, while in CT the dose distribution has an approximate circular symmetry. Examples of Monte Carlo (MC) simulated dose distributions from the two modalities are shown in Figure 2.4.

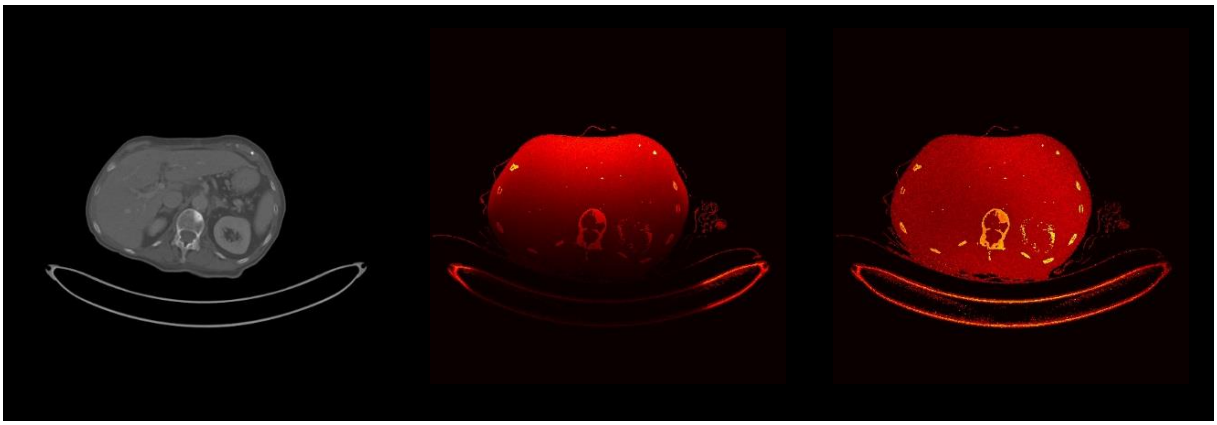

Figure 2.4. A CT image (**left**) and Monte Carlo simulated dose distributions from projection radiography (**middle**) and CT (**right**). The patient is from **Paper V**.

In the 1970s, the CT dose index (CTDI) was introduced [20], where CTDI is the average dose in a central position of a volume. The $CTDI_{100}$ is the CTDI over a length of 100 mm, calculated using the following equation:

$$\mathrm{CTDI}_{100}\ [\mathrm{mGy}] = \frac{1}{N \cdot T} \cdot \int_{-50\ \mathrm{mm}}^{50\ \mathrm{mm}} D(z)\,\mathrm{d}z\,, \tag{2.2}$$

where $N \cdot T$ is the collimation of the scan and $D(z)$ is the dose profile along the scan direction where z is the position. CTDI can be measured free in air, although typically it is measured in a circular polymethyl methacrylate (PMMA) phantom that corresponds to the head or the body (diameters of 16 cm and 32 cm, respectively). The length of the phantom should be at least 14 cm [21], typically 14 or 15 cm. Weighted CTDI ($\mathrm{CTDI_W}$) is calculated using the following equation:

$$\mathrm{CTDI_W}\ [\mathrm{mGy}] = \frac{1}{3} \cdot (\mathrm{CTDI_C} + 2 \cdot \mathrm{CTDI_P}), \tag{2.3}$$

where $\mathrm{CTDI_C}$ and $\mathrm{CTDI_P}$ are the $\mathrm{CTDI_{100}}$ measured in the PMMA phantom centrally and peripherally, respectively. This metric is straight-forward to determine and represents a simple estimate of the average CTDI over the axial plane. To take patient table motion into account, $\mathrm{CTDI_{VOL}}$ is used. For axial scanning it is defined as:

$$\mathrm{CTDI_{VOL}}\ [\mathrm{mGy}] = \frac{N \cdot T}{\Delta d} \cdot \mathrm{CTDI_W}, \tag{2.4a}$$

where Δd is the distance of the patient table between consecutive scans. For spiral scanning $\mathrm{CTDI_{VOL}}$ is defined as:

$$\mathrm{CTDI_{VOL}}\ [\mathrm{mGy}] = \frac{\mathrm{CTDI_W}}{p}, \tag{2.4b}$$

where p is the pitch (Equation 2.1). The $\mathrm{CTDI_{VOL}}$ is one of two dose indices that are presented with every examination in CT. The other is the dose length product (DLP), which is the $\mathrm{CTDI_{VOL}}$ multiplied by the scan length L:

$$\mathrm{DLP}\ [\mathrm{mGycm}] = \mathrm{CTDI_{VOL}} \cdot L\,. \tag{2.5}$$

The DLP relates to the total absorbed energy during the CT scan. Note that the $\mathrm{CTDI_{VOL}}$ and DLP are not measures of the dose to the patient, but measures of the dose to a standardized PMMA phantom. Further, the $\mathrm{CTDI_{VOL}}$ and DLP depend on the phantom size and, thus, care should be taken when discussing dose index values. In CT scanners, a prediction of the CTDI and DLP is presented before the actual scan, giving the CT technologist an indication of the dose level.

There are three main methods for estimating CT patient dose; E/DLP conversion factors, MC pre-calculated conversion factors and MC simulated estimations.

The E/DLP conversion factors are convenient and simple to use: the factors are multiplied by the DLP of the scan. It is important to note for which phantom the conversion factors are valid for. The most commonly used set of factors are those from the American Association of

Physicists in Medicine (AAPM) [22]. Since those types of factors are developed to cover a broad range of CT scanners and a generic patient model, such factors are coupled with substantial uncertainties.

A more flexible and reliable method is to use pre-calculated MC conversion factors [23]. This method is often built into software packages. When using those the user specifies the CT scan conditions, whereupon the software presents organ doses and an effective dose.

The third and most complicated CT dose estimation method is to use direct MC simulations. It is challenging to model a CT scanner and an object (patient or phantom). However, when that has been achieved, the method is flexible and modification of scan parameters or the object is simple. There have previously been studies published where the patient table was included in the MC estimations, although the effect of including or neglecting it was not mentioned [24-26].

2.3 IMAGE QUALITY

In CT, an axial image is built up by a matrix of 2D pixels, typically 512x512. In three dimensions (3D), this corresponds to an axial image where the thickness in the z-dimension corresponds to the slice thickness. The simplest method to reconstruct a CT image is to use back-projection (BP). Each projection from the scan is divided evenly along each projection back on to the 2D matrix. The problem with this approach is that all projections pile up, resulting in a blurred reconstruction. It can be compensated for by deconvolution of each projection with a filter, a method called filtered BP (FBP). The choice of filter depends on the user's preference of image quality. It is an important decision for the image quality as it introduces a tradeoff between noise and spatial resolution. The reconstruction filter (also called kernel by some vendors) is selectable in the CT scanner console. In Figure 2.5, an example of the visualization of three circular objects by BP and FBP is shown.

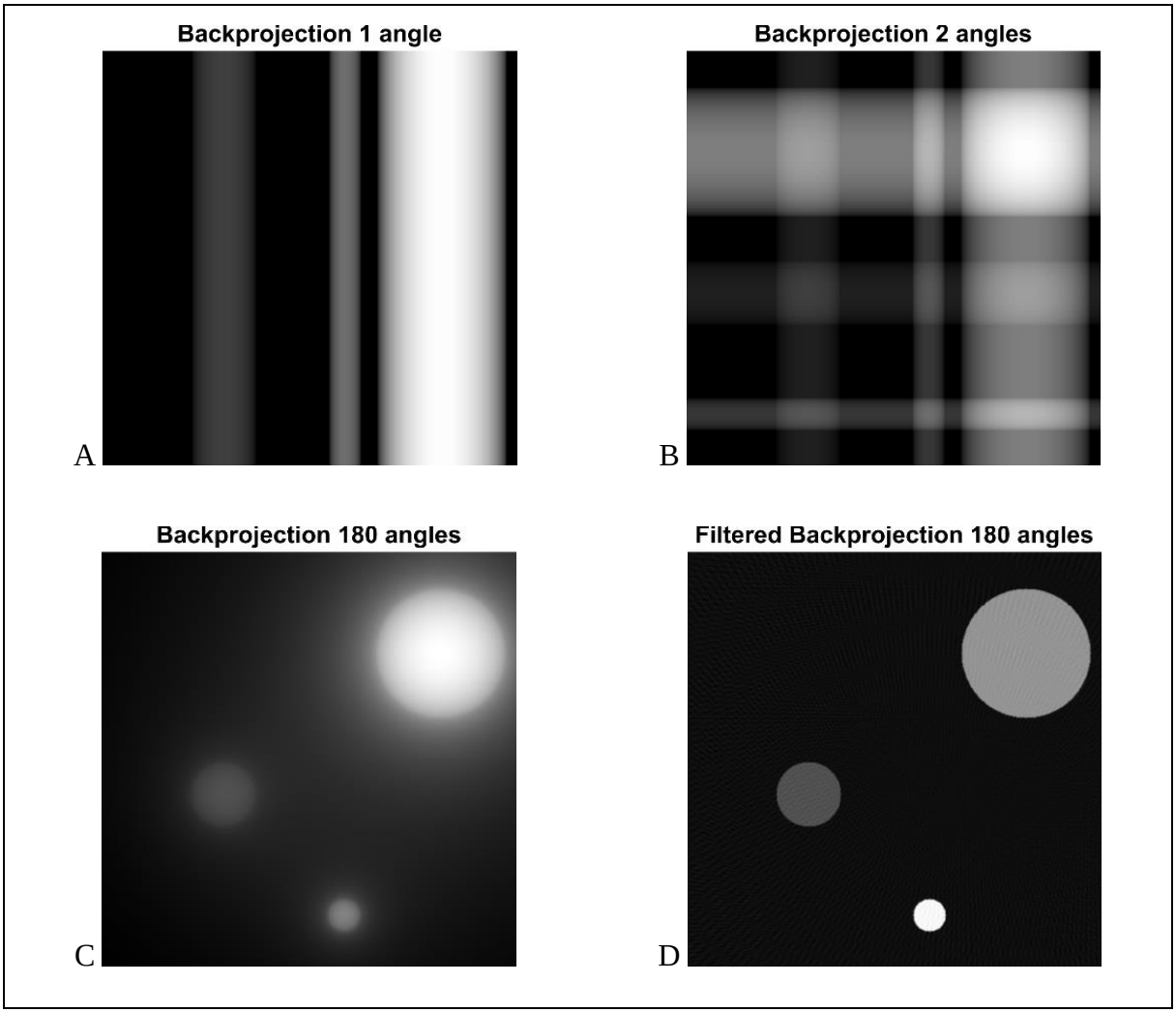

Figure 2.5. Demonstration of back-projection (BP) and filtered BP (FBP). (**A**) and (**B**) are images reconstructed with BP using only 1 and 2 projections respectively. (**C**) and (**D**) are image reconstructed using BP and FBP using 180 projections. The filter used in the FBP reconstruction was a Ram-Lak filter. Figures created using MATLAB (version r2019b, MathWorks Inc., Natick, MA).

The reconstruction technique that was used in the first CT scanners was an iterative reconstruction (IR) technique, called algebraic reconstruction technique [27]. Reconstruction with FBP is done using a single step, while IR produce a CT image with multiple repetitions that converges towards a good solution. It is a computationally demanding task, and it is not until lately that it is starting to be commonly used, mainly because of the increase in available computer power. The reconstruction process starts with an estimation of the image (commonly an FBP image), which is forward projected into artificial raw data. The artificial raw data is compared to the measured raw data to create a correction term that is applied to the estimation of the image. This method is iterated until a predefined criterium is reached (e.g. a number of iterations). The IR method can be made advanced with incorporated models of the scanning geometry and photon statistics. In principle, more advanced models require more computational power. [28]

The use of IR has advantages compared to FBP, the images are created with lower noise and less artifacts. The lower noise leads to an improved low contrast resolution. Consequently, while maintaining image quality, the radiation dose can potentially be lowered. However, the image characteristic is different compared to FBP, which comes from that the algorithm is

non-linear. The spatial resolution is dependent on the contrast and noise of the surrounding tissues. To target this problem, CT scanners typically provide a choice on how aggressive the IR should be. Further, due to the non-linearity of IR algorithms, simple image quality metrics such as standard deviation are insufficient to quantify the resulting image quality. Efforts are being taken to develop model observers to quantify the effectiveness of IR [29].

In 2019, a new type of CT image reconstruction was released on the market, deep learning reconstruction (DLR), including AiCE (Canon Medical Systems, Otawara, Japan) and TrueFidelity (GE Healthcare, Waukesha, WI, USA). The image is reconstructed (recovered) using a deep convolution neural network [30]. The DLR algorithm relies on data that it has been trained with, which consists of high dose FBP images. The training data is used to find image "features" that build the image. When measured raw data has been analyzed, the DLR is able to find features it has learned from the training to build a CT image, even when the raw data comes from a low-dose scan. This method is not as computational demanding as IR, once the training phase is completed, which makes DLR more feasible to use.

Figure 2.6 contains a CT image acquired in a CT scanner that supports DLR (Canon Aquilion One Prizm Edition, Canon Medical Systems, Otawara, Japan). It was acquired using 100 kV, a $CTDI_{VOL}$ (32 cm) of 1.7 mGy, a slice thickness of 0.5 mm and reconstructed with FBP, IR and DLR.

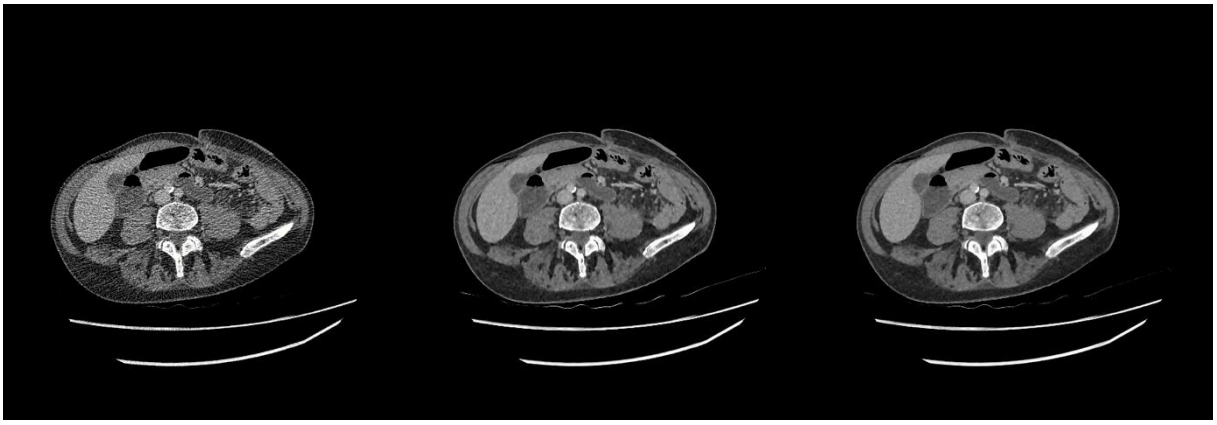

Figure 2.6. CT image reconstructed with (**left**) filtered back projection, (**middle**) iterative reconstruction (FIRST, Canon Medical Systems, Otawara, Japan) and (**right**) deep learning reconstruction (AiCE, Canon Medical Systems, Otawara, Japan). Courtesy of Luuk Oostveen, Radboudumc, Nijmegen, The Netherlands.

Image quality in CT can be divided in several components: noise, low contrast resolution, high contrast (spatial) resolution and z-axis resolution (slice thickness). These components, together with radiation dose, are connected in a complicated way and are often investigated during CT optimization in QAC groups.

Image noise is the uncertainty of the pixel value (CT number), σ, in a homogenous region. It comes from various sources: random statistical noise and systematic fluctuations, from either the radiation emission and transmission, the detection, the reconstruction or from anatomy in the patient that is not part of the examination. In CT, the image noise is defined as the standard deviation of pixel values in a ROI. The ROI size and placement are important factors to consider when measuring noise.

The noise level in CT images is related to the statistics of the underlying data. Brooks' formula [31] (rewritten by Nagel [32]) can be used to predict how some parameters will affect the noise level:

$$\sigma^2 \propto \frac{e^{-\mu d}}{D \cdot a^2 \cdot b \cdot T}, \tag{2.6}$$

where $e^{-\mu d}$ is the attenuation of the object with the thickness d, D is the radiation dose, *CTDI*, a^2 is the sampling distance, b is the collimation and T is the slice thickness. Noise squared, σ^2, is the variance. The peak tube voltage (V_P, usually denoted by the unit kV) dependence can be predicted by using $D \propto V_P^n$, which is how the radiation dose varies with V_P, with n being a CT scanner dependent factor, which is typically around 2.6 [33]. Further, the tube current (I, usually denoted by the unit mA) and rotation time (t, usually denoted by the unit s) can be inserted due to their linear dependence on dose, D. The noise level then becomes:

$$\sigma^2 \propto \frac{e^{-\mu d}}{I \cdot t \cdot V_P^n \cdot a^2 \cdot b \cdot T}. \tag{2.7}$$

The visual appearance of noise can differ drastically depending on the noise texture, i.e. the spatial frequency distribution of the noise. The use of standard deviation as a metric has limitations as it will only measure the overall level of noise. To measure how noise, both the level and texture, propagates through the CT system, the noise power spectrum (NPS) can be used. It describes how the noise in one point of the system is correlated to the noise in the surrounding points of the image [34]. The NPS can be determined by calculating the Fourier transform of an ROI in a uniform image that only contains noise.

In CT, most examinations require a good low contrast resolution, usually called "image contrast". It is the ability to resolve objects with small differences in attenuation ("low contrast" objects). A brain examination is an example where a low contrast resolution is needed to distinguish between gray- and white brain matter.

Typically, low contrast resolution is measured as the CT number difference between the tissue of interest and the background. However, this measure does not take into account that the noise level has a great impact on the ability to distinguish between the two tissues. An alternative measure that does take this into account is the contrast-to-noise ratio (CNR), which is the previously mentioned CT number difference divided by the noise in the background.

High contrast resolution, also called spatial resolution, is the ability to resolve small ("high contrast") objects. The choice of reconstruction filter is important as it will decide the level of spatial resolution. A reconstruction that yield an image with a high spatial resolution, will also result in a relatively high level of noise. However, the noise level can be prospectively handled by adjusting the dose to a desired level. Another way of improving the spatial resolution is by decreasing the reconstruction field of view, because of its linear dependence with the pixel size.

The spatial resolution is either quantified by measuring how many line pairs per distance can be distinguished (measured in a phantom with different amount of line pairs), or by measuring the modulation transfer function (MTF). The MTF is a measure of how well an imaging system is able to process signals of different spatial frequencies through the image chain. The MTF is often measured in a CT image of a wire (approximately a point). A line-spread function (LSF) is calculated from a profile of the point, and the MTF is calculated as the Fourier transform of the LSF.

It is important to identify the contrast requirements for any CT-protocol. For examinations requiring a good high contrast resolution, a higher level of noise is acceptable, as the window settings are chosen with a wide range of CT numbers included. A consequence is that such examinations can be performed with lower radiation doses. For such cases, techniques like CT scanning with tin filtration can be used by optimizing the spectra, through removal of low-energy photons [35].

The z-axis resolution is the slice thickness of the image. A small slice thickness will result in an image with a high noise level and a good (z-axis) resolution where small object can be distinguished. Vice versa, a larger slice thickness results in lower noise and worse resolution. To quantify this, the effective slice thickness can be measured with a slice sensitivity profile (SSP). The SSP can be measured by scanning a ramp with a known angle.

The SSP is of interest in current generation of CT scanners where spiral scan technique is widely used, as interpolation is required to get full projection data for CT image reconstruction. The selected pitch of the acquisition will influence that interpolation. A high pitch CT scan results in worse SSP compared to a low pitch CT scan.

3 QUALITY ASSURANCE (PAPER I)

In Sweden, the commonly used QA scheme for CT is according to earlier national regulations, stating that a QC of a CT scanner should be performed at least annually [36] and each time a change has been made that affects the image quality or radiation dose [36, 37]. In institutions with a large number of radiological equipment these requirements imply that a large part of medical physicists' time is devoted to performing QCs. At Karolinska University Hospital (in year 2012), annual QC of a CT scanner took two days: one day for measurements and one day for analysis. Further, many of the tests included were user dependent, for example due to manual ROI placements. It has been recommended that objective methods should be developed for image analysis [38, 39]. In 2018, the Swedish Radiation Safety Authority (Strålsäkerhetsmyndigheten, SSM) published new national regulations where it was stated that QCs should be performed to the extent and time interval deemed to be necessary to ensure a safe radiological equipment [10].

There are also recommendations for more frequent QCs. The American College of Radiology states that CT numbers and noise should be tested daily [40] and the International Electrotechnical Commission (IEC) states that noise, CT numbers and uniformity should be tested at least monthly [41].

In **Paper I**, a methodology to reduce the number of technical parameters to test at the QC was developed at Karolinska allowing them to be evaluated within the daily QA program, internally referred to as "MonitorCT". This could be achieved by using the concept of key performance indicators (KPIs). A KPI is a parameter that depends on many underlying and more fundamental parameters. The idea was that when a KPI is out of the tolerance range, it is caused by an underlying parameter being out of range. That parameter can be found by using relevant subsequent test. This concept is common in manufacturing industries. Suitable KPIs can be inferred by scanning the manufacturer's QA phantom which is delivered with each new CT scanner. In **Paper I** multiple KPIs were identified: positioning, image noise, CT numbers of water and air, uniformity and homogeneity (Table 3.1).

Table 3.1. CT parameters generally tested during quality assurance (QA) and their dependency on key performance indicators.

Parameters tested during QA (A = acceptance, C = constancy)		**Parameters dependency on key performance indicators**	
Direct tests	Image noise (A, C)	***Image noise***	***CT Numbers***
LASER accuracy (A, C)	Uniformity (A, C)	X-ray tube voltage	CT number of water
Tabletop indexing (A)	Inter-slice noise (A, C)	$CTDI_{VOL}$	CT number of air
Tabletop orientation (A)	Geometric accuracy (A)	$CTDI_{AIR}$	Calibration
Scan plane localization (A, C)	Spatial resolution (A, C)	Spatial resolution	
$CTDI_{VOL}$ (A)	Scattered radiation (A)	HVL	***Positioning***
$CTDI_{AIR}$ (A, C)	System documentation (A,C)	Low contrast resolution	Tabletop indexing
Dose-noise response (A)	Radiation protection documentation (A, C)	Collimation	Tabletop orientation
Dose-noise linearity (A)	Radiation shielding (A, C)	Slice thickness	Scan plane localization
X-ray tube voltage (A, C)	Radiation notification (A, C)	Geometric efficiency	
HVL (A, C)	Staff interview (C)	Z-dose profile	***Uniformity***
Z-dose profile (A)	Artifact evaluation (A,C)	Dose-noise response	Shaped filter
Geometric efficiency (A)		Detector response	Reconstruction
CT number of air (A, C)	***Indirect tests***	Inter-slice noise	Detector
CT number of water (A, C)	Shaped filter		
CT numbers of various materials (A, C)	Calibration	***Homogeneity***	
CT number linearity (A, C)	Dose display (A,C)	Artifact evaluation	
Slice thickness (A, C)			

The ROI size and placements for the analysis of noise, CT number of water and uniformity were chosen in accordance with IEC recommendations (Figure 3.1) [41, 42]. The homogeneity KPI was introduced to identify artefacts that otherwise could be undetected, such as a ring artefact placed outside the uniformity ROIs.

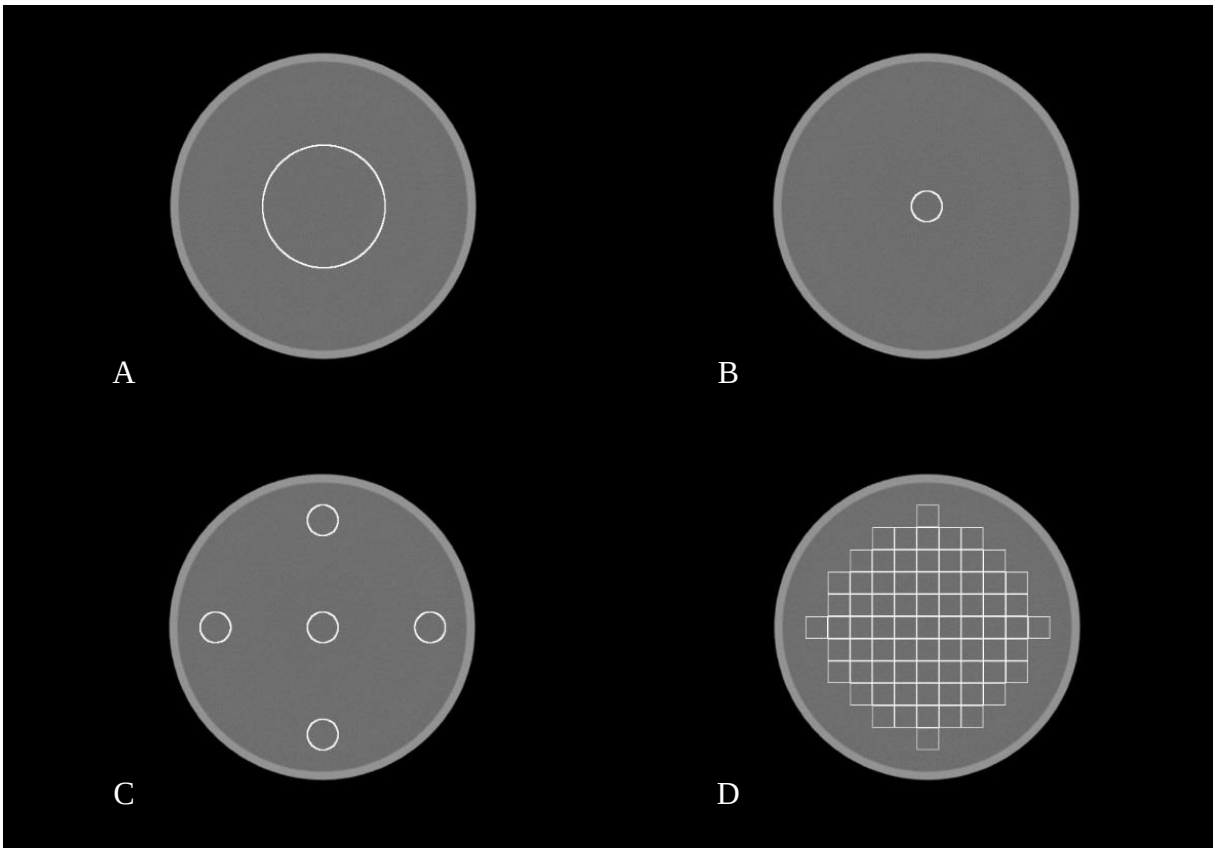

Figure 3.1. ROI placements in the analysis of water in the MonitorCT application: (**A**) noise, (**B**) CT number of water, (**C**) uniformity and (**D**) homogeneity.

By creating an automated workflow for the KPI analysis, constancy tests could be performed without disrupting the clinical workflow. The simplified tests could be designed to be easily performed by CT technologists in combination with a standard morning calibration. Two levels of testing were defined (level 0 and level 1) with fixed scan parameters for reproducibility and possibility for trend analysis. The idea was to keep level 0 as simple and short as possible enabling quick daily checks. The level 1 test was designed to have multiple scans with all available scan parameters varied systematically. Figure 3.2 illustrates the workflow used at two CT scanners at Karolinska University Hospital's Neuroradiology clinic.

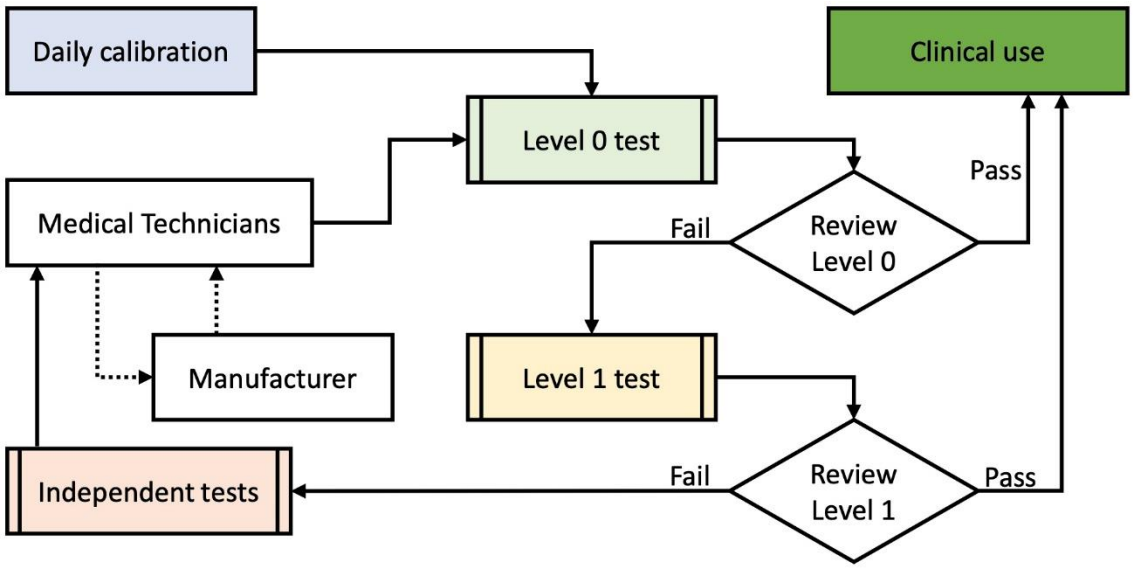

Figure 3.2. Flow chart of the proposed routine QC methodology.

During the past six and a half years MonitorCT has been running at two CT scanners. In total, results outside of tolerances has been discovered at 10 occasions: one case of increased noise and nine cases of CT numbers out of range. The failed noise test was due to a ring artefact, which subsequently was attributed to dirt in the tube collimator housing (Figure 3.3).

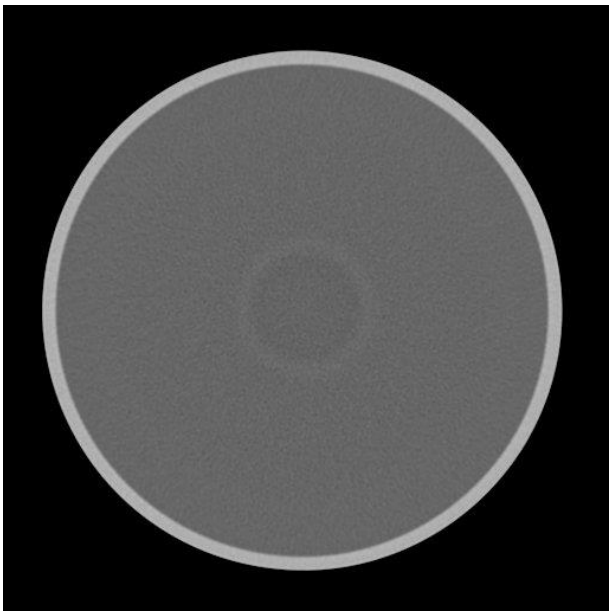

Figure 3.3. CT image with a ring artefact discovered with the noise test.

Unfortunately, the homogeneity test failed to detect the ring artefact, indicating poor sensitivity for this type of malfunction. The CT number trend for the two CT scanners is shown in Figure 3.4 (one CT scanner was replaced during this time). The multiple deviations that were discovered turned out to be due to a "bug" in the CT scanner software of the specific CT scanner model (Figure 3.4, but not the old CT 1).

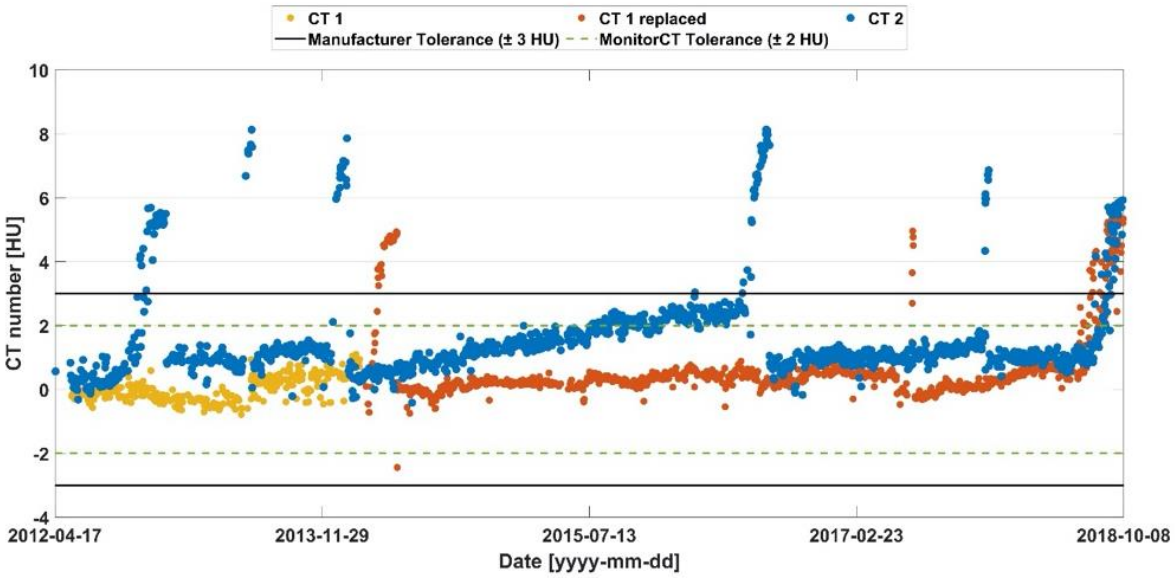

Figure 3.4. CT number trends for two CT scanners at a radiology clinic. CT 1 was replaced during year 2014 (yellow = old CT 1, red = new CT 1, blue = CT 2).

The feedback from the clinic has been positive; MonitorCT provided confidence that the technical status of the CTs was under control. For the medical physicist, this methodology has also shown the feasibility of a new type of trend analysis that has not been possible previously.

4 AUTOMATIC TUBE CURRENT MODULATION (PAPER II)

Most CT scans are performed using ATCM. It is a function which aims at keeping a homogenous image quality throughout an examination and among patients. It is defined by a parameter called image quality reference parameter (e.g. GE uses noise index which is a definition of the desired noise level). ATCM was introduced clinically in 1994 [43] and consists of two parts: angular modulation and z-axis modulation. Usually these parts are combined. The angular modulation is designed to keep a constant detector signal during a rotation, while the z-axis modulation aims at keeping a certain level of dose/image quality along the patient in the z-direction [44]. Since its introduction, various manufacturers have implemented ATCM based on different principles. It has been previously shown that there is a need for CT personnel (radiologists, CT technologists and medical physicists) to understand ATCM and the differences among various manufacturers' implementations [45, 46], but this is challenging. There are studies that have investigated how the ATCM adapts with specific parameters [45, 47-54] but an extensive characterization had not been performed previously. Unexpected results had been reported [47], and it had been noted that a comparison of various ATCM techniques among vendors was lacking.

The aim with **Paper II** was to develop a method of characterizing the ATCM and to characterize the ATCM of the four recent CT scanners from the four major CT vendors (GE, Philips, Siemens, Toshiba) in Sweden. The investigated CT scanners were: GE Revolution CT (GE Healthcare, Waukesha, WI, USA), Philips Brilliance iCT 256 (Philips Healthcare, Eindhoven, The Netherlands), Siemens SOMATOM Force (Siemens Healthcare, Forchheim, Germany) and Toshiba Aquilion One Vision Edition (Toshiba Medical Systems, Otawara, Japan). The vendors' specific implementations of ATCM are described in the paper. Commercially available phantoms for ATCM characterization were imperfect at the time of writing [47, 50, 51, 55, 56]. The two most common limitations were sharp edges ("wedding cake" design) and the lack of homogenous areas of the phantom. A sharp edge can result in fluctuating tube current values in proximity to the edge. The lack of homogenous parts (in the z-direction) does not allow ATCM to stabilize. For the evaluation of ATCM, a phantom was developed to avoid those limitations and a method to characterize the ATCM response was proposed. The phantom was commercialized (The Phantom Laboratory, Salem, NY, USA) and is now available for everyone working in the field. The schematics and pictures of the developed phantom are shown in Figure 4.1. Specifically, the design goals for the ATCM phantom were:

- uniform material to reliably measure noise,
- wide sections for spiral collimations up to 80 mm,
- different sized sections for longitudal modulation,
- elliptical cross sections for angular modulation,
- smooth transitions between consecutive sections.

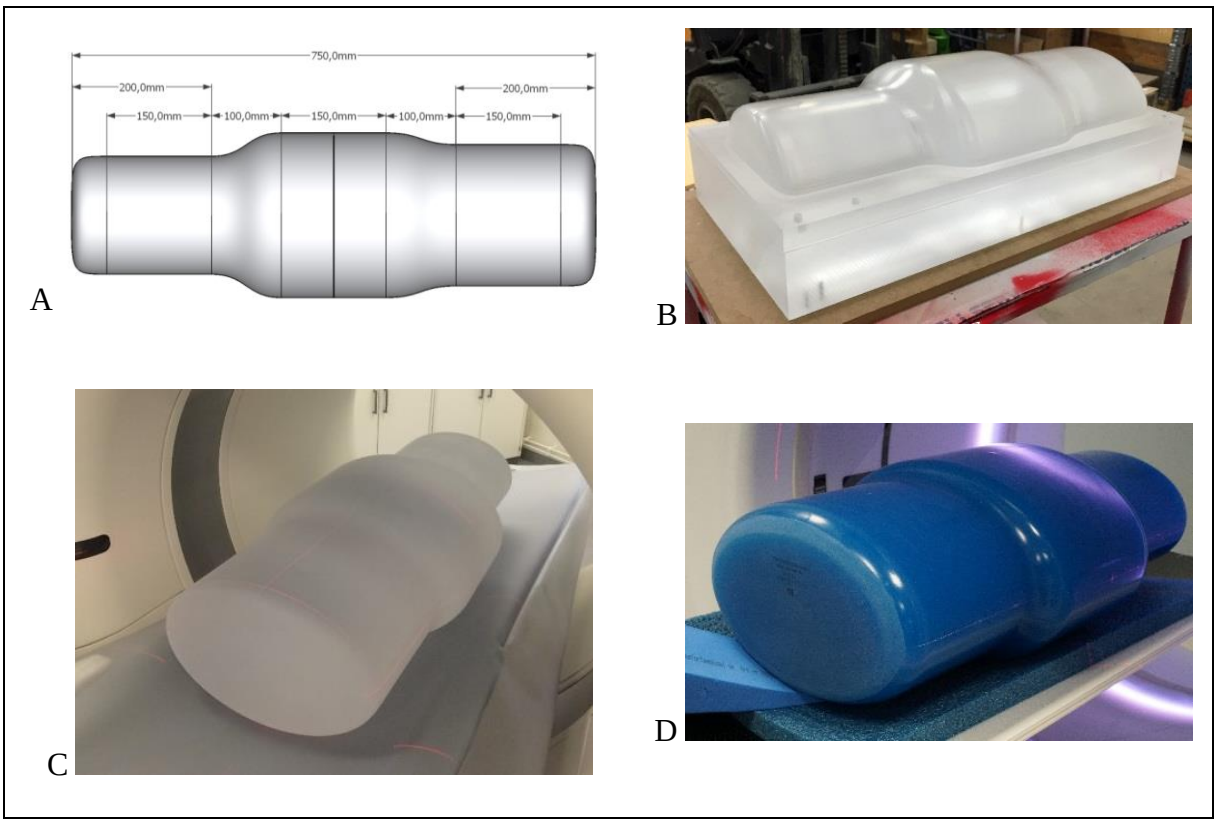

Figure 4.1. The developed automatic tube current modulation phantom from **Paper II**. The phantom schematics from the side (**A**). The phantom was milled from a solid piece of PMMA (**B**). The prototype phantom used for measurements (**C**) and the commercially available phantom (**D**).

To characterize the ATCM, a standardized scan was defined and then repeated with one scan setting systematically varied at a time. The resulting data consisted of multiple scan series that could be analyzed with regard to tube current and noise. Each image in each series was individually analyzed by acquiring the meta data of the image (DICOM header) for the tube current information and performing an image analysis for noise calculation using the pixel data. Figure 4.2 shows the ATCM response from varying the image quality reference parameter of the investigated CT scanners. The varied scan parameters also included those available for LR acquisition and for image reconstruction. Further, in addition to scan parameters, the phantom centering was varied.

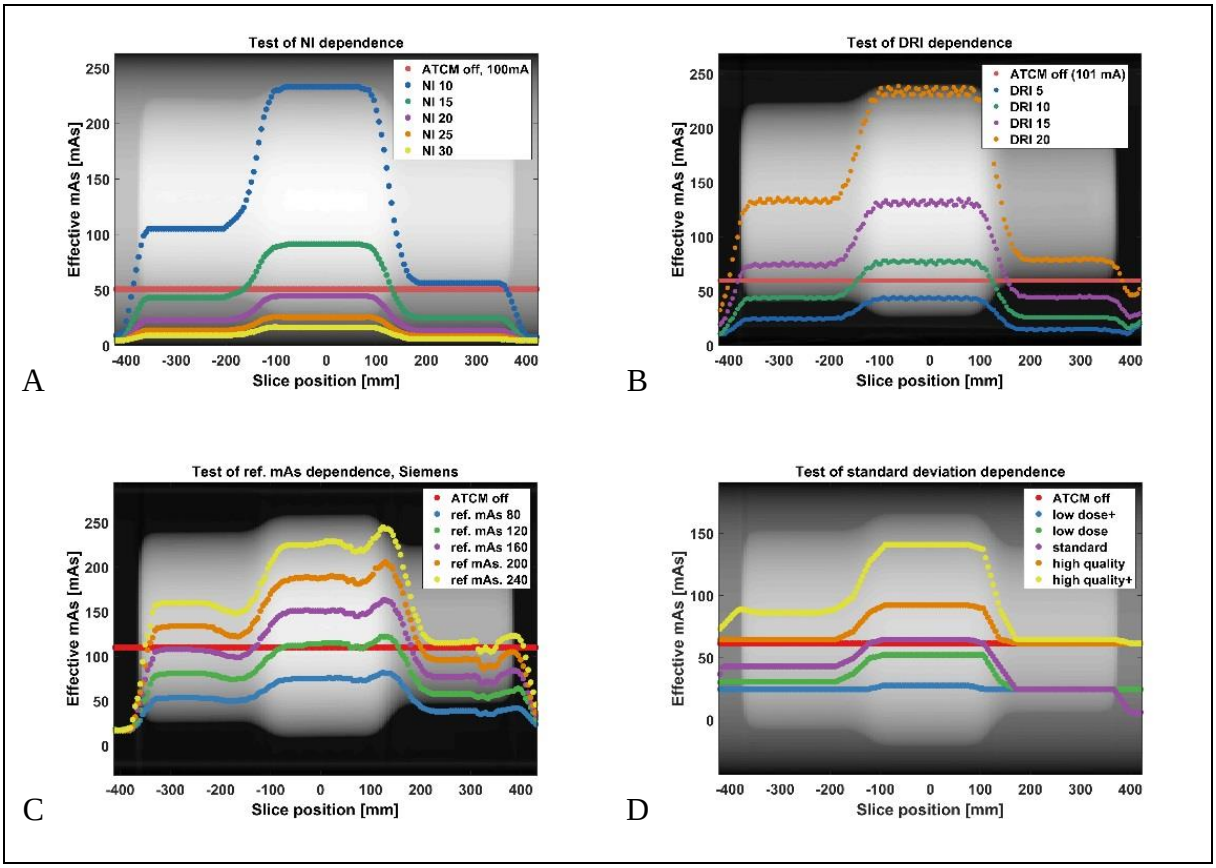

Figure 4.2. The automatic tube current modulation response from varying the image quality reference parameter in CTs from GE (**A**), Philips (**B**), Siemens (**C**) and Toshiba (**D**).

To determine whether a scan parameter change was affecting the ATCM, the normalized root mean squared error (NRMSE) was calculated between the modified and the standard scan. A change was deemed to affect the ATCM if the NRMSE exceeded two times the NRMSE for two identical standard scans. The study resulted in tabulations of data showing how scan parameters affect the ATCM for the investigated CT scanners. Three groups of varying scan parameters (tables) were created: LR parameters, scan parameters and reconstruction parameters. It is difficult to place the patient perfectly in the center of the CT scanner. This can be a problem as miscentering affects image quality adversely [57, 58]. Therefore, beyond the mentioned tables, a separate table for miscentering parameters was created.

Figure 4.3 demonstrates how the ATCM responded to the use of an LR with varied tube voltage for two different CT scanners: one exhibited a varying response and the other a constant response. This implies that for some CT scanners it is not advisable to use the lowest possible kVp of the LR to reduce dose as the ATCM of the full scan will be affected. Also, it was shown that the investigated CT scanners' ATCM functions could not handle LRs obtained with low dose. In Figure 4.4, the ATCM is shown for a CT scanner with a consistent response at higher tube voltage (120 kV) regardless of tube current strength, but with a diminishing response at low tube voltage (70 kV) when the tube current is decreased.

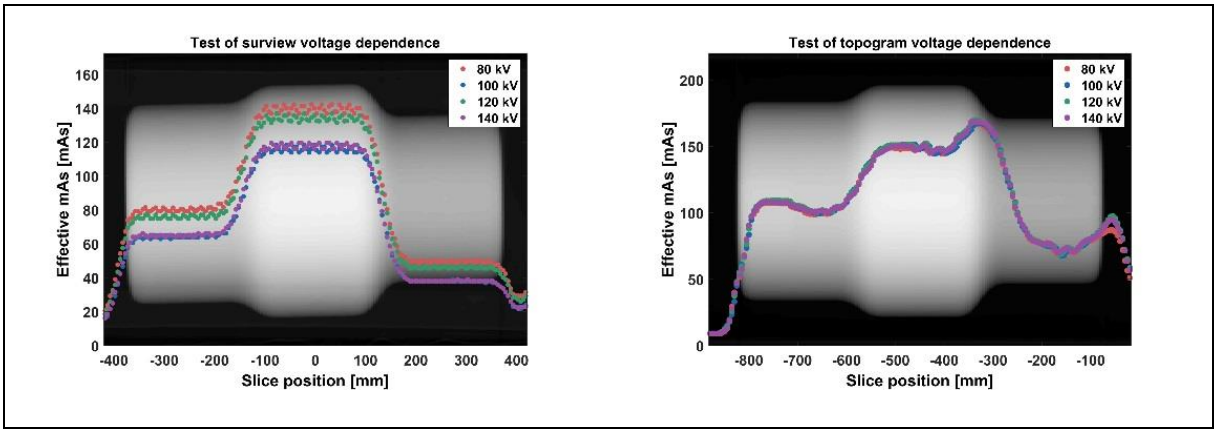

Figure 4.3. The automatic tube current modulation response from varying the tube voltage of the localizer radiograph obtained using a CT from Philips (**left**) and Siemens (**right**).

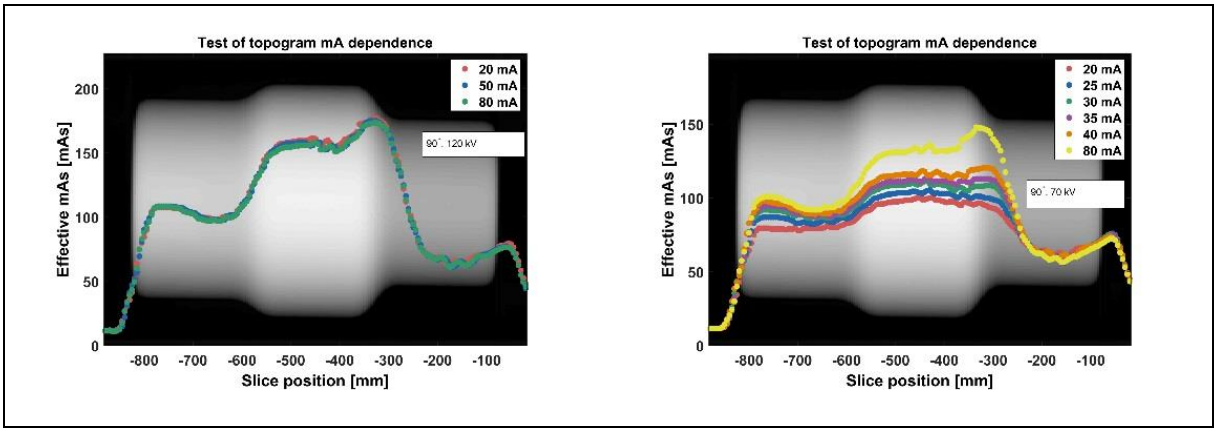

Figure 4.4. The automatic tube current modulation response from varying the tube current of a lateral localizer radiograph acquired with 120 kVp (**left**) and 70 kVp (**right**) in a Siemens CT.

The ATCM used by Siemens currently combines z-axis modulation and angular modulation. The angular modulation is varied on the fly ("online"), based on detector signals obtained in earlier stages of the scan spiral. More specifically, it uses the information from the previous half rotation (signal from the opposite side). The z-axis modulation on the other hand, is adjusted in advance. A different approach is used by GE, where the LR is used to define both the angular and z-axis modulation. In clinical practice, the differences in z-axis modulation can be of importance. For example, when performing a thorax examination on a Siemens equipment, it is preferred to scan from superior to inferior, so that the CT has ramped up the tube current before scanning the diaphragm, to avoid too low tube current which would result in worse image quality. The ATCM principle currently used by GE avoids this issue (Figure 4.5).

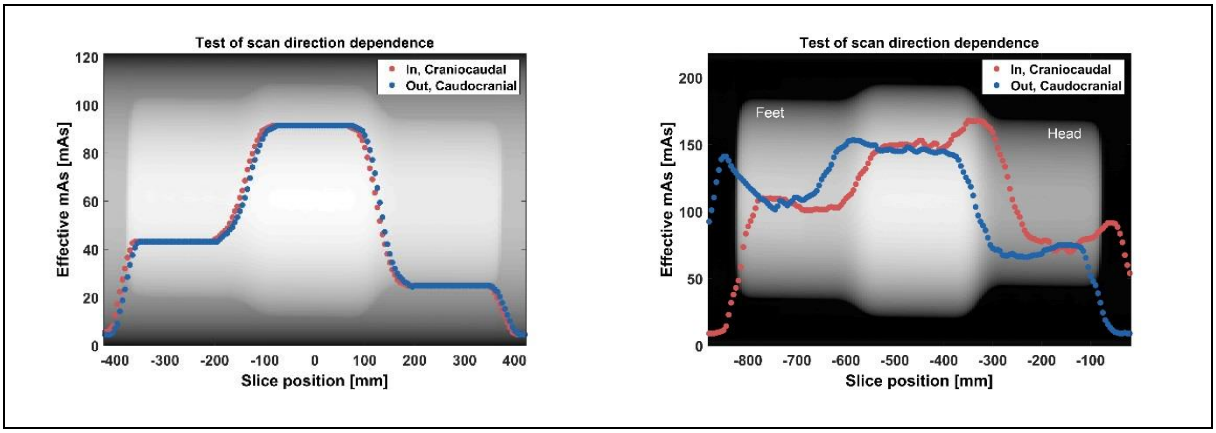

Figure 4.5. The automatic tube current modulation response from varying the scan direction in a CT from GE (**left**) and Siemens (**right**).

The ATCMs from Philip and Toshiba did account for the patient table height, while the ATCMs from GE and Siemens did not; see Figure 4.6 for a comparison of the ATCM from Philips and Siemens. Note that this does not mean that patient centering is of less importance in Philips and Toshiba CT scanners. The effect on image quality and dose due to the shaped filter must still be considered, despite a consistent ATCM response. Good patient centering is always important for enabling optimal image quality.

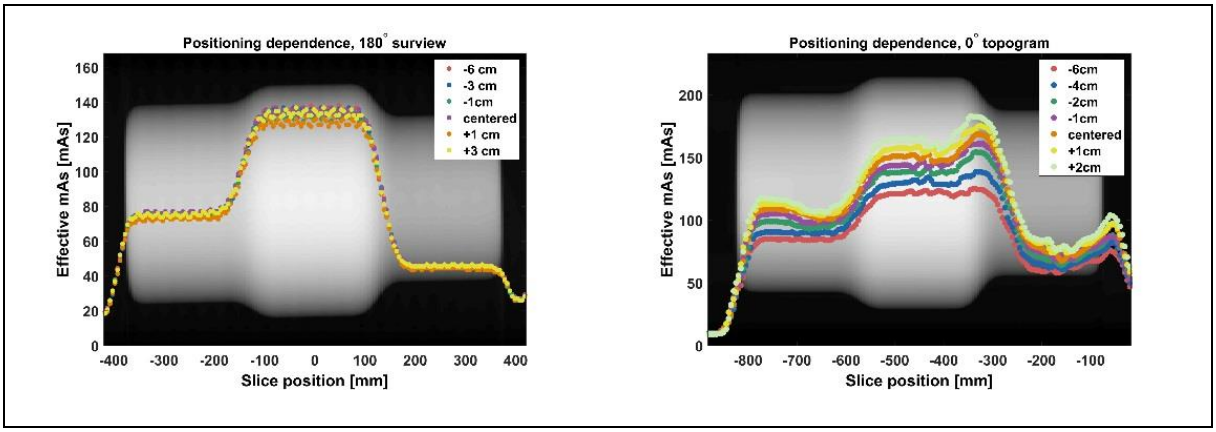

Figure 4.6. The automatic tube current modulation response from varying the patient table height in a Philips (**left**) and Siemens (**right**) CT.

There were large differences among CT manufacturers in how ATCM was affected by the tested parameters. Moreover, CT scanners from the same vendor could have different ATCM implementations depending on the CT scanner model and software.

5 DOSIMETRY INCLUDING THE PATIENT TABLE (PAPER III)

Common software packages that uses pre-simulated MC conversion factors include CT-Expo (version 2.2, Medizinische Hochschule, Hannover, Germany) and ImPACT CT Patient Dosimetry Calculator (version 0.993, Imaging Performance Assessment on Computed Tomography, www.impactscan.org). These software packages do not take the patient table into account and it has been unclear how a patient table in CT affects the estimation of patient doses. In patient dose estimations in radiology, an accuracy (expanded uncertainty, k=2) of 7% is appropriate [59]. When performing the study in 2017 there was only one previous publication on the impact of neglecting the patient table in CT dose estimations: the Monte Carlo dataset from the National Radiological Protection Board (NRPB) in the UK, which was published in 1991. It reported effective dose differences between 2% and 6% when the patient table was excluded [60]. It was not stated to which technique those findings applied. Modern CT scanners are able to perform spiral scans at doses comparable with conventional projection radiography [29], while the dose from an LR can be substantial in low-dose scans. This should be taken into account when computing the total dose to the patient [61]. LRs are often acquired with the X-ray tube stationary at 6 o'clock (below the patient). In those cases, the impact from the patient table is of special interest. The aim of **Paper III** was to investigate the patient table effect on patient dose estimations.

The commercial MC simulation software ImpactMC (AB-CT Advanced Breast-CT GmbH, Erlangen, Germany) was used to simulate LRs with the X-ray tube at different angles and a spiral scan, with and without the patient table. Three different patients were simulated: the ICRP 110 male and female voxelized phantoms [62] and the GSF voxelized phantom child [63]. The patient table was added into the simulations from a segmented CT scan of a real table. The material of the table was set equivalent to muscle (in accordance with one CT vendors' recommendations[1]) and with density empirically adjusted. A simulated dose volume in the ICRP 110 female voxelized phantom (including the patient table) from an LR acquired with the X-ray tube stationary at 12 o'clock is shown in Figure 5.1. The effect of the shaped filter can be seen, as the dose is higher in the central part of the X-ray beam.

[1] Personal communication with Siemens Healthcare

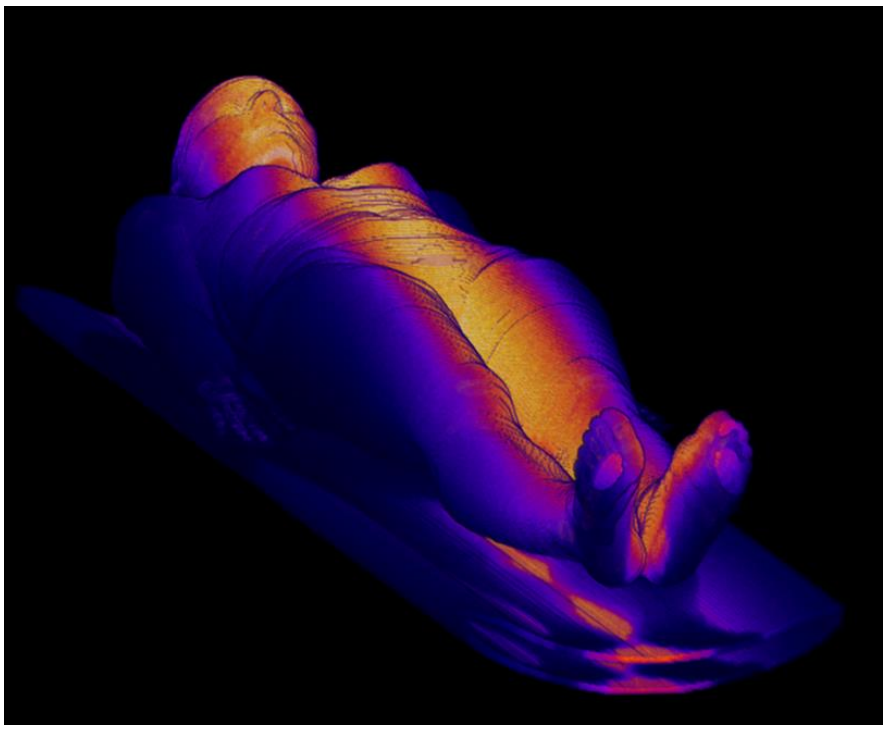

Figure 5.1. Dose volume from a Monte Carlo simulation of a CT localizer radiograph of the female voxelized phantom, including the patient table.

After scanning, the acquired data volume of the voxelized phantom was segmented to analyze the dose volumes from the simulations. It could be shown that the radiation dose is overestimated when the radiation absorption of the patient table is not included in the radiation dose estimations. The effective dose is overestimated by 5% for spiral scans and 14-23% for LRs acquired with the X-ray tube stationary at 6 o'clock. For LRs acquired with the X-ray tube stationary at 12 o'clock, the effective doses were underestimated by up to 1%, because of backscattering. The overestimation for spiral scans agrees with the MC dataset from the NRPB which stated that effective dose differences were between 2% and 6% [60].

6 LOW-DOSE SPIRAL SCANS FOR CT SCAN PLANNING

Modern CT examinations can be performed at very low doses [35, 61, 64]. In this chapter, the focus is on two future areas where low-dose spiral scans can be implemented for CT scan planning: as a replacement of the conventional LR and for intravenous CM dosage planning.

6.1 SCAN PLANNING (PAPER IV)

The concept of LR was introduced in the end of 1970s to help planning CT scans [65]. Since then, the concept of CT scan planning has not changed much. The main disadvantage with the use of LRs is that the displayed patient geometry is highly affected by the patient positioning. This occurs due to the diverging geometry since the X-ray beam is in the shape of a fan. Because of this, objects closer to the X-ray tube will give a greater shadow on the detector than objects further away from the X-ray tube. As shown in **Paper II**, some CT scanners can keep the tube current constant when an object is miscentered, but not able to adjust the patient table to the optimal height to account for the shaped filter.

By performing a low-dose spiral scan; it is possible to create a 3D map of the scanned object. In a previous publication it had been shown how such a 3D map can be used for selecting the correct scan volume for a subsequent CT scan with higher quality [66]. However, current scanners in principle require an LR for the scanning. By projecting the obtained 3D volume at any direction it is possible to form a LR-like image [67], a so-called synthetic LR, SLR. By creating an SLR, it should be possible for manufacturers to implement the technique of low-dose 3D CT planning to current CT scanners with minor effort. There are also some more theoretical advantages of using a low-dose spiral scan for CT scan planning; it would allow automatic scanning with an automatically selected field of view, scan length and patient centering. In most CT scanners, a spiral scan is faster to acquire than an LR. This means that the workflow would be faster, especially since many clinics use two LRs for CT scan planning. **Paper IV** was an investigation of the feasibility of the implementation of SLRs for CT scan planning.

The first step of the investigation was a dosimetric comparison of a spiral CT scan acquired at the lowest possible radiation dose and LRs acquired from three angles. The same dose estimation method (by means of MC) as in **Paper III** was used**,** although simulating a different CT scanner. The scan range of the dose estimation was selected to include the whole patient (scan from above the head to below the feet). The estimated radiation doses are shown in Table 6.1. As shown in **Paper II**, the radiation dose of an LR cannot be used with lowest possible output from the X-ray tube because it results in noisy LRs that can adversely affect the ATCM or image quality. Hence, when calculating the radiation dose from the LRs the default scan settings (for the simulated CT) were used, according to vendor recommendations.

Table 6.1. Estimated effective doses from a spiral scan and LR with the X-ray tube stationary at 12 o'clock (LR-AP), 3 o'clock (LR-LAT) and 6 o'clock (LR-PA), for a patient positioned supine.

	Spiral (SLR)	**LR-AP**	**LR-LAT**	**LR-PA**
Effective dose [mSv]	0.14	0.14	0.06	0.07

The effective dose was equal for the low-dose spiral scan (SLR) and the LR with the X-ray tube stationary at 12 o'clock. However, the most common combination of LRs at Karolinska (and probably elsewhere) is two LRs: with the X-ray tube stationary at 3 and 6 o'clock, respectively. This combination still results in approximately the same radiation dose as the low-dose spiral scan (SLR). Note that the SLR can be created at an arbitrary angle at no additional radiation dose. This could be used for patients that cannot be positioned prone or supine, for example due to contractures.

The SLR is created by calculating the mean CT number in the desired projection. This is done without the beam divergence, eliminating any magnification effects. In this study, the patient table was digitally removed prior to the calculations.

Altogether, SLRs were created for ten patients undergoing thorax-abdomen CT examinations by scanning with an additional low-dose spiral scan. The LRs and SLRs were blinded and evaluated by 4 experienced radiologists and 2 experienced CT radiographers. In total, 4 scan ranges were compared, 3 ranges obtained on anterior-posterior images (length of the lung, lung apex to pubic symphysis and thinnest part of patient) and 1 range obtained from the lateral images (broadest part of the patient). The ranges were compared using independent t-tests. Further, the image quality was evaluated using a side-by-side relative visual grading, where the SLR was graded relative to the corresponding LR on a 5-scale grade with the following scores: 1 clearly superior, 2 somewhat superior, 3 equal, 4 somewhat inferior and 5 clearly inferior. These results were analyzed by calculating a confidence interval (CI) of the mean using t-test statistics [68, 69]. Figure 6.1 show examples of LRs and SLRs of a patient.

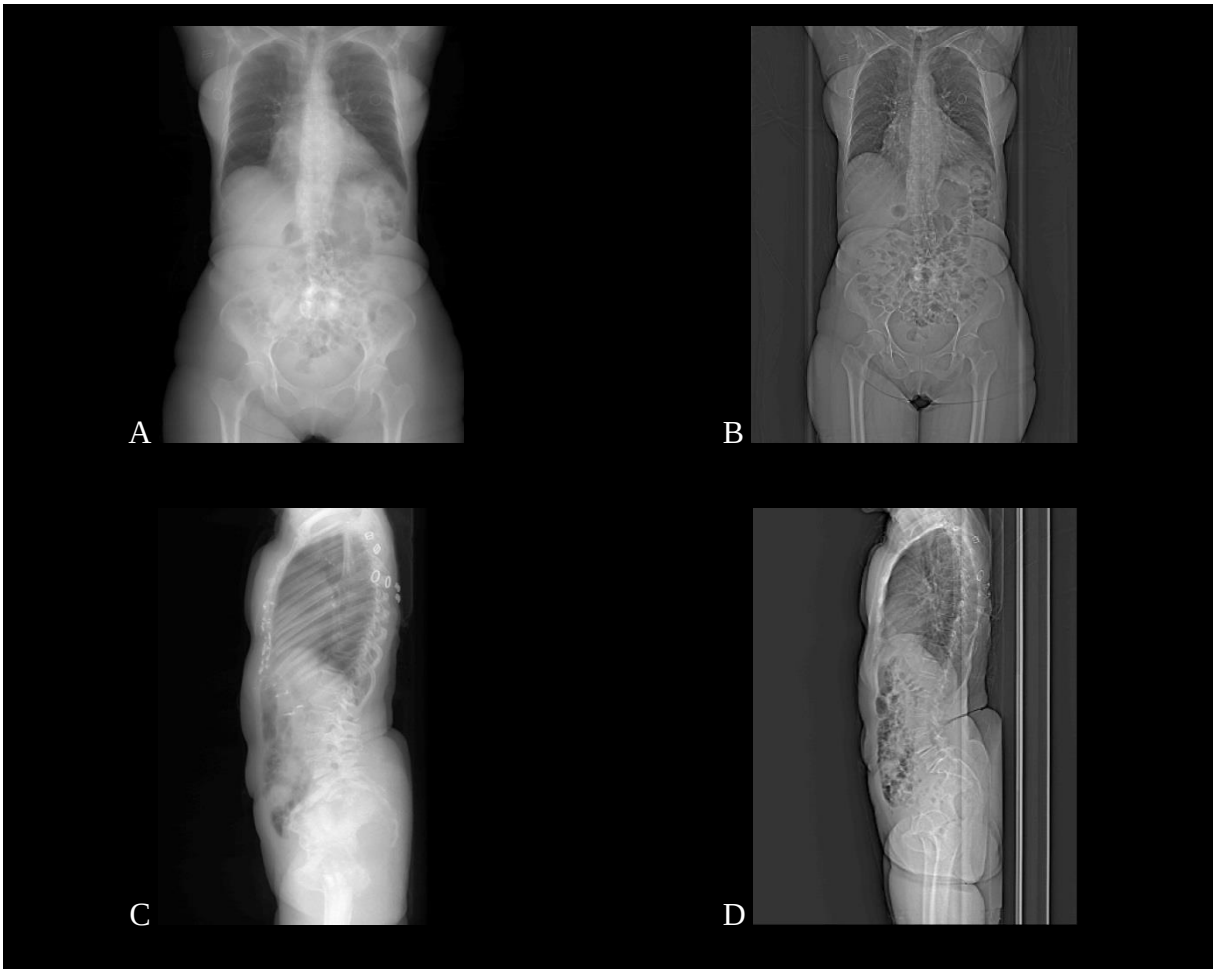

Figure 6.1. A set of localizer radiographs of a patient (female, 73 years old). (**A**) and (**C**) shows synthetic localizer radiographs reconstructed from a low-dose spiral scan in the anterior-posterior and lateral direction, respectively. (**B**) and (**D**) shows an anterior-posterior and a lateral localizer radiograph, respectively.

There was no significant difference in the measured lengths obtained from the anterior-posterior images (p=0.06 to 0.84), while there was a significant deviation in the width of the broadest part of the patient measured on the lateral images (p<0.001), with a mean difference of 18 mm. The image quality of the SLRs reconstructed in the anterior-posterior direction was rated superior with a mean score of 2.5 (CI: 2.2-2.9), while the lateral SLR had a mean score of 3.3 (CI: 2.7-3.9), i.e. no significant difference.

The geometrical effect on the LR and the SLR was investigated by scanning the ATCM phantom centered (the commercial version of the phantom from **Paper II**), 3 cm mis-centered and 6 cm mis-centered. The water equivalent diameter (WED) was acquired from the DICOM header of the LRs [70] and followed by image analysis of the low-dose spirals [71], with and without the patient table. The estimated WEDs of the centered phantom and 6 cm mis-centered phantom were compared using t-tests. Figure 6.2 shows the WEDs of the small and large part of the ATCM phantom.

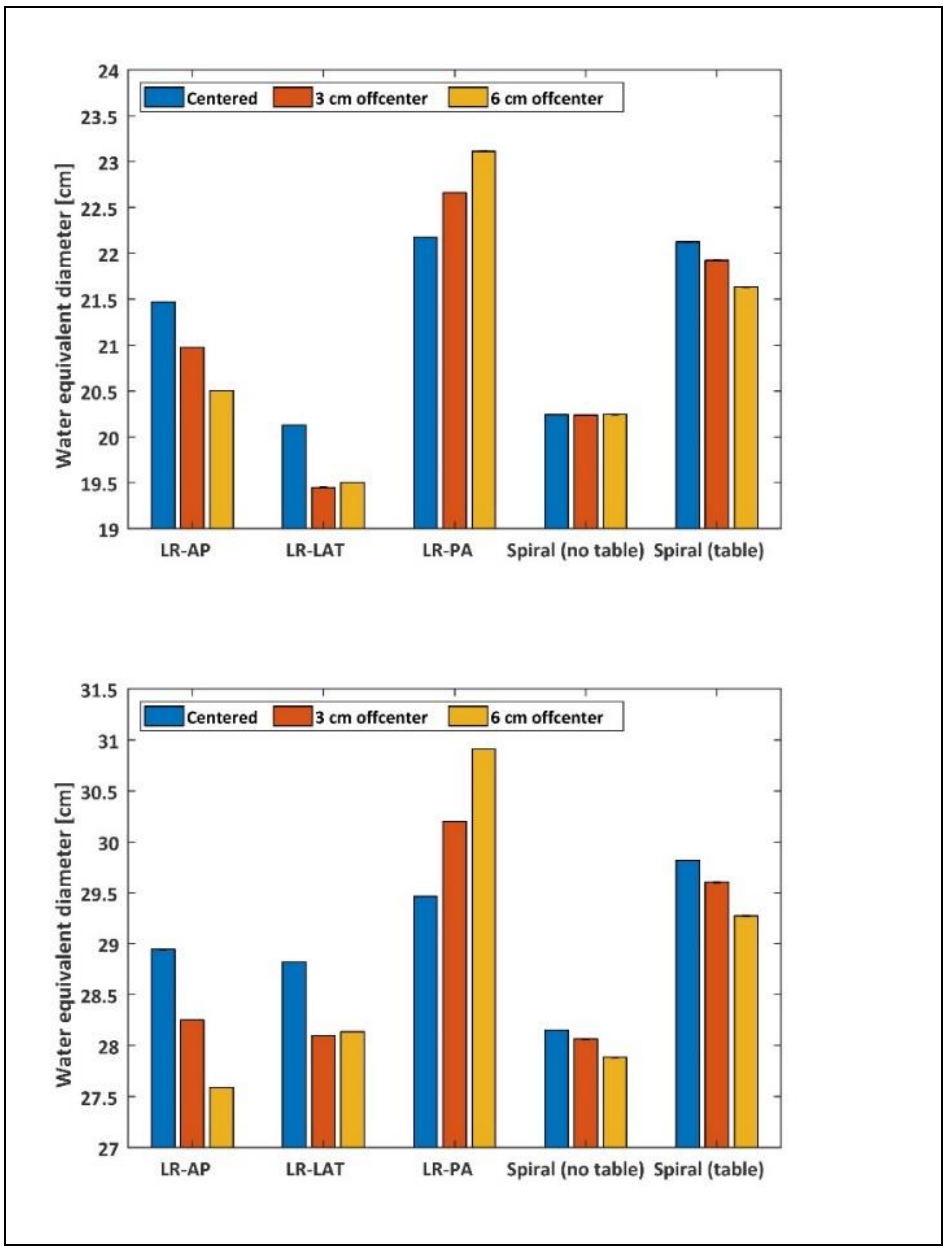

Figure 6.2. Water equivalent diameter of an automatic tube current modulation phantom for localizer radiographs acquired with the X-ray tube stationary at 12 o'clock (LR-AP), 3 o'clock (LR-LAT), 6 o'clock (LR-PA) and calculated from a spiral scan with and without a patient table. Small part of the phantom (**up**) and large part of the phantom (**down**).

No statistically significant variation of estimated WEDs could be shown for a spiral scan without the patient table in the small section of the phantom (p=0.87). However, the same could not be said for the large section of the phantom (p<0.001), although the magnitude of difference was only 0.3 cm. The largest variations of WEDs came from the LRs with the X-ray tube stationary at 12 o'clock and 6 o'clock (1-1.4 cm, p<0.001), followed by the LRs with the X-ray tube stationary at 3 o'clock (0.6-0.7 cm, p<0.001).

These results indicate that the WEDs are more accurately estimated from low-dose spiral scans with the patient table digitally removed and that the LR angle has an impact on the ATCM. For the most consistent function of the ATCM, it should therefore be planned from a volume of the patient. We did not further investigate the ATCM as we did not have access to any vendors' ATCM algorithm. Nevertheless, this work showed that the implementation of a low-dose spiral CT (as an SLR) is feasible for CT scan planning.

6.2 INTRAVENOUS CONTRAST MEDIA DOSAGE PLANNING (PAPER V)

In CT, most of the examinations are performed using intravenous CM to better visualize anatomy and pathology in the human body. By adjusting the CM dosage and timing, the imaging of the enhancement can be planned to occur in different contrast phases. An example of a contrast phase is the early arterial phase, where the CT examination is performed when the CM is still in the arteries. Another example of a contrast phase is the portal venous phase, where the liver parenchyma is optimally enhanced to distinguish between normal liver and low-vascularized lesions, optimally with a liver enhancement of at least 50 HU [72]. Factors that will influence enhancement are CM dose, CM timing and the scan protocol settings. While the CT number enhancement is linear with CM dose [73], the use of a fixed dose is still a common clinical practice implying that large patients are under-dosed and small patients over-dosed [74]. An under-dose results in insufficient enhancement which makes diagnosis difficult, while an over-dose can lead to acute kidney injury. Instead of using a fixed CM dosage scheme, an individualized scheme can be used [72, 75, 76]. The most common variable for individual CM dosage planning is body weight (BW) (gram iodine per kg BW) [73]. Some studies suggest using the lean body mass (LBM) [77], which is the fat-free weight. Notably, the use of BW has limitations, since CM enhancement in the fat is smaller than in visceral organs and muscular tissue. Thus, larger patients also risk over-dosing with such a dose scheme [73, 78]. In **Paper V**, the low-dose spiral scan for CT scan planning was further investigated. The patient's body volumes of muscular tissue (V_{MUSCLE} [dm^3]) and fat tissue (V_{FAT} [dm^3]) were calculated from the low-dose scan and its potential for CM dose planning was evaluated. Four CM dosage models were investigated; (1) BW, (2) BW and body height (BH), (3) LBM or (4) the V_{MUSCLE} and V_{FAT}. Further, the influence from gender was examined.

At PET/CT, an attenuation correction CT (ACCT) is obtained after the conventional LR to correct PET data for the patient's body size and composition. This ACCT is a low-dose non-diagnostic CT scan similar to the low-dose scan that was used for creating the SLR in **Paper IV**. At Karolinska University Hospital the PET scan is most often followed by a diagnostic CM enhanced CT scan. In this project, 262 PET/CT examinations including CM were retrospectively analyzed. Several patients were excluded:

- nine patients were scanned with a deviating tube voltage,
- eleven patients who had arms in the field (one or two arms down),
- nine patients who had no CM enhancements in the liver,
- three patients who had CM enhancement in the liver deemed as outliers (more than three standard deviations from the mean).

After these exclusions, 238 patients were included (88%, 118 men, 120 women). For each patient, the BW, BH, the CM dosage and the CT images were acquired. The patient body volumes were calculated by analyzing the 3D volume of the ACCT between the top of the lung and the pubic symphysis. This region was chosen to compare equivalent regions among patients. Further, a 5x5x5 3D median filter was applied for smoothing the 3D volume to

reduce noise. Lastly, CT number thresholding [17] was used to segment the V_{MUSCLE} and V_{FAT}. A "non-specified" volume was segmented to include parts in the 3D volume that are not of interest (e.g. the lung volume). For each patient, the CT number enhancement was measured as the difference between CT numbers in a ROI in the liver in the diagnostic scan and the ACCT, carefully avoiding filled vessels in the diagnostic scan.

Multiple linear regressions were made using the CM dose divided by the CT number enhancement in the liver as the dependent variable. The second-order Akaike information criterion (AIC_C) was calculated for each model comparison [79, 80]. This is a metric for relative performance of different models where a smaller AIC_C indicates a better fit. For each model comparison, the AIC_C weight was also calculated [81], which is the probability that the model is best among the compared models. Models with an AIC_C weight >0.95 were considered significantly better than the others. Because of the relative comparison, it is desirable to compare a small number of models (to determine a clear "winner"). The investigated CM dosage models were investigated including gender, which showed that it is a significant variable for all regressions ($p<0.05$) except using LBM ($p=0.22$).

The first comparison which was made was among models with (1) BW and (2) BW and BH. The models had similar fit, with AIC_C weights of 0.44 and 0.56, respectively (adjusted R^2 values of 0.43 and 0.44). As the use of BW alone is simpler, this model was selected for the next stage of model comparison: between (1) BW, (3) LBM and (4) the V_{MUSCLE} and V_{FAT}. The outcome was that the best model for CM dosage is using the V_{MUSCLE} and V_{FAT}. The adjusted R^2 of the BW model was lower, although the difference was not large (BW adjusted R^2=0.43 versus V_{MUSCLE} and V_{FAT} adjusted R^2=0.48). Therefore, both resulting equations were presented for the intravenous CM dosage as a function of desired CT number enhancement (HU) and the gender ($gender_{NUM}$), with the assignments men=0 and women=1. The BW and LBM performed similarly and, therefore, only the BW equation was shown (LBM is more complicated to calculate):

$$\text{CM dose} = HU \cdot \left(0.6594 + 0.014892 \cdot BW - 0.22825 \cdot gender_{NUM}\right), \quad (5.1)$$

$$\text{CM dose} = HU \cdot \left(0.46892 + 0.052065 \cdot V_{MUSCLE} + 0.021209 \cdot V_{FAT} - 0.15956 \cdot gender_{NUM}\right). \quad (5.2)$$

The regressions of (1) BW and (4) the V_{MUSCLE} and V_{FAT} are shown in Figure 6.3. The variation among the patients is large, indicating that predicting CM dosage is a difficult task which needs further investigation. Based on these results, it was shown that it is feasible to plan the CM dosage with the patient's volumes of muscle and fat calculated from a low-dose scan. Due to the small theoretical improvement we would not recommend acquiring a low-dose scan only with the purpose of CM dosage planning. In such cases, it should be preferable to continue the use of BW. However, in patients undergoing a diagnostic CT after their PET the new paradigm should be beneficial.

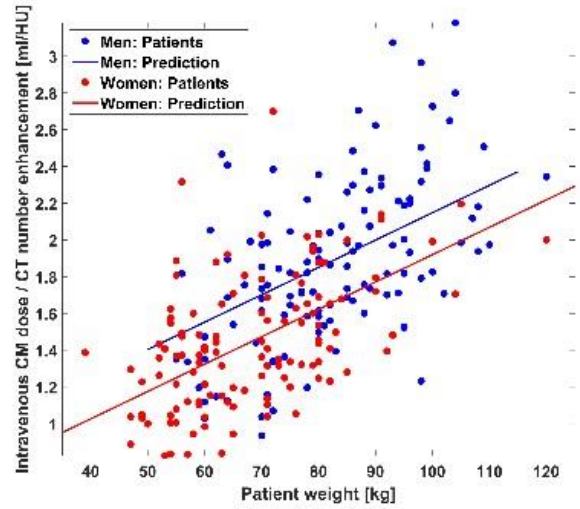

A

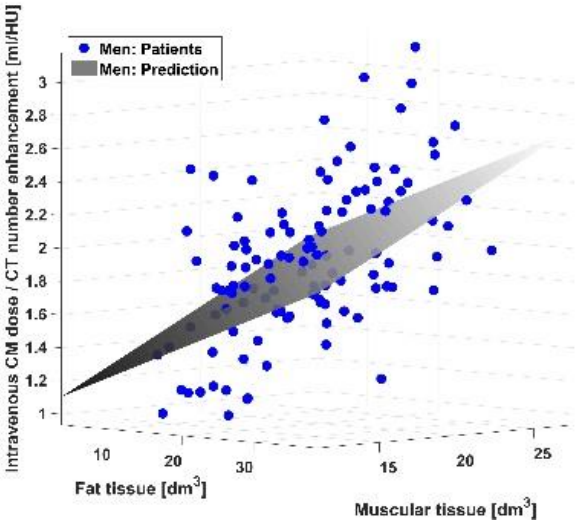

B

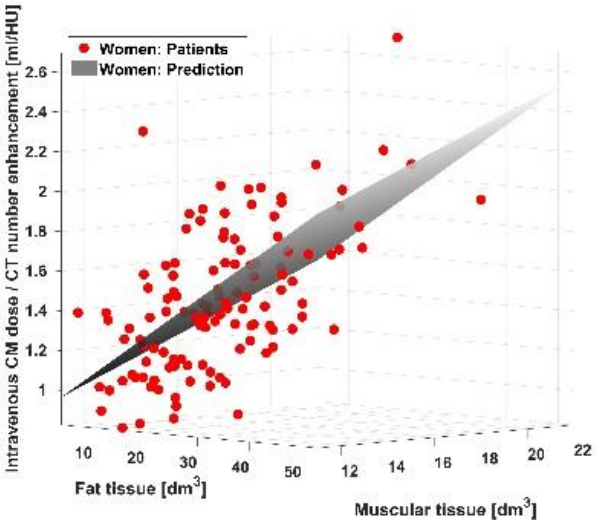

C

Figure 6.3. Regressions of intravenous contrast media divided by CT number enhancement in the liver and (**A**) body weight (adjusted R^2=0.43) and body volumes of muscle and fat (adjusted R^2=0.48) for men (**B**) and women(**C**).

An important factor to consider in CM dosage planning is the maximum CM dosage. This was not taken into account in the equations of this study and should be considered in an eventual implementation. Figure 6.4A shows how the CM dosage (for a fixed CT number enhancement in the liver) can be predicted using the pertinent equation with BW. The prediction curves for CM dose continue beyond the maximum CM dosage used in the routine scheme. Further, Figure 6.4B shows that the limit on CM dosage used in the current clinical scheme used for the study results in decreased liver CT number enhancement for the heaviest patients.

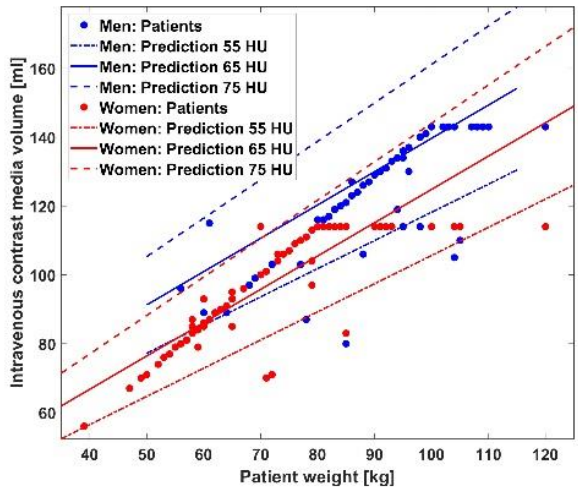

A

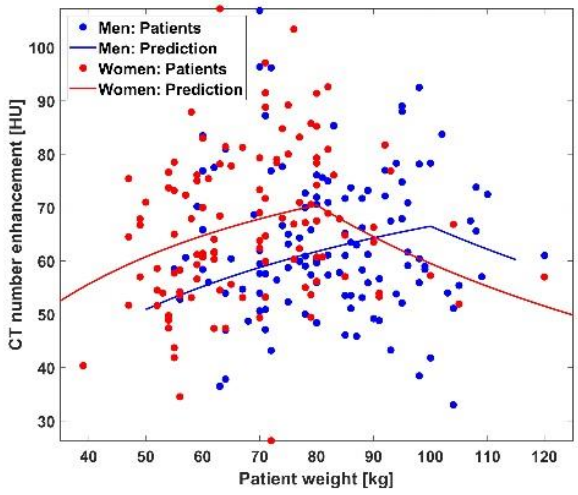

B

Figure 6.4. Intravenous contrast media dose (**A**) and CT number enhancement in the liver (**B**) versus body weight. The predicted curves for intravenous contrast media dosage are made at three levels of CT number enhancement in the liver: 55 HU, 65 HU and 75 HU. The prediction of the CT number enhancement in the liver is made using the routine contrast media scheme.

7 CONCLUSIONS

This Thesis has yielded a set of results and tools that can help radiology clinics and manufacturers in improving CT examinations.

The fundamental requirement for a radiology clinic with CT is a well-functioning CT scanner. In **Paper I**, a methodology of performing quality controls was presented, which allows for daily automated QCs, using the concept of key performance indicators. Further, the approach facilitates trend analysis, enabling detection of emerging problems.

Paper II resulted in a phantom and a method for comprehensive characterization of the automatic tube current modulation. Additionally, the ATCM was characterized from the latest (at the time of the study) CT models from four major CT manufacturers, which showed differences depending on the model and software.

In **Paper III**, it was shown that the patient table is an important factor to consider when estimating radiation dose to the patient.

Based on image quality, radiation dose and geometric accuracy, **Paper IV** demonstrated that it is feasible to use a synthetic localizer radiograph created from a low-dose spiral scan for CT scan planning, replacing the traditional localizer radiograph.

Based on a retrospective study in **Paper V**, it was shown that intravenous contrast media dosage can be planned using patients' muscular and fat volumes extracted from a low-dose CT scan.

This Thesis has demonstrated that optimizing the quality at CT scanning is complex, and that further research is needed in each of the investigated areas: CT scanner performance, ATCM, low-dose scans and intravenous contrast media dosage. However, the tools and techniques developed and presented here are steps forward. It is hoped that the results will be of use and interest to healthcare professionals in the field, such as in quality assurance committees, as well as the wider community of researchers and manufacturers.

8 FUTURE ASPECTS

During this project multiple insights have emerged that should be investigated further.

In **Paper I**, two levels of these tests were defined: daily (level 0) and extended (level 1). The level 0 test was shown to find multiple deviations, while the level 1 test has not yet been evaluated fully. The idea was that a level 1 test can be used to further pinpoint a potential aberration. However, the abnormalities that were discovered during the study could be pinpointed using the level 0 test alone. It would also be of interest to include more advanced physical image quality metrics, such as MTF and NPS in the daily test bundle. Some of the tests could also be improved, especially the homogeneity and the positioning test.

Automatic tube current modulation algorithms should be further investigated and optimized (**Paper II**). For example, techniques to characterize the angular modulation and automatic tube voltage selection should be developed.

Paper III could be expanded investigating different CT scanners and different patient tables, to assess the variations in effect of the patient table on dose between vendors and scanner models.

Building on **Paper IV**, it would be of interest to investigate whether the 3D volume of the patient can be used as an input data to the automatic tube current modulation to optimize both tube current and tube voltage. Further, it should be determined whether a clinical implementation of the synthetic localizer radiograph concept could be achieved using the software of a CT scanner.

A prospective study is ongoing where the contrast media dosage planning equation (**Paper V**) including the patients' muscular and fat volumes is used. However, a study should be done investigating whether the relationship found by regression can be used on other CT scanners. Further, this study could be expanded to include pediatric patients.

With the upcoming introduction of photon counting detectors on the CT market, it should be investigated how the ability to identify contrast media will affect clinical workflow and contrast media doses.

Another topic that should be investigated is the introduction of algorithms implementing artificial intelligence (AI), such as deep learning algorithms. In quality controls of radiological equipment, an AI could identify performance trends. In the future, it is probable that an AI algorithm will optimize CT scan protocols and CT scanning. Already today, some vendors have the functionality for automatic adaptation of CT scan protocols depending on patient characteristics, e.g. if the patient has metal parts in the body or if the patient has a fast heart rate. Further, there are vendors that have AI powered algorithms for improved automatic segmentation of the body and it should be investigated whether this can aid in contrast media dosage planning.

ACKNOWLEDGEMENTS

During my PhD-studies, I have encountered a lot of amazing people who have inspired me and have taught me valuable lessons. Without them, I would not have managed to make it. I want to especially thank the following persons and groups.

My main supervisor Torkel Brismar: for providing an excellent base for my PhD-studies and for guiding me through the process. You always see solutions, although it seems impossible. You have always had time for me (even standing in the middle of a ski slope).

My co-supervisor Gavin Poludniowski: for all helpful discussions and for all your help and guidance on the way. I cannot keep track of the number of documents and methods you have helped me with, always with great remarks and insights.

My mentor Sven Nyrén: for your guidance, for encouraging me to start my PhD-journey and for putting me in contact with Torkel.

Robert Bujila: I am grateful for our time at Karolinska. I want to thank you for all the collaborations and discussions and for that you always believe everything is possible.

Deborah Merzan: for your support and the excellent work during your time in the CT group. Although you have moved on to new challenges, I will always see you as a CT physicist!

Annette Fransson Andreo: for creating and maintaining the research-friendly environment at the X-ray department at Karolinska University Hospital.

Dževad and Karen Belkić: for your support and valuable comments on the thesis.

Lena Gordon Murkes: for your support and for always being available for discussions.

The departments of pediatric radiology and neuroradiology at Karolinska University Hospital: for always welcoming me at your CT scanners, allowing me to perform tons of scans and measurements. I have always felt as an integral part of your respective teams.

Melina Auvinen: for being my biggest supporter, always providing me with whatever I need and for always being there for me.

My family: for always supporting me and for providing the stable foundation that is so important in life.

REFERENCES

1. Röntgen, W., *Über eine neue Art von Strahlen.* Gesellschaf, Würzburg, 1895. **137**: p. 132-141.
2. Mould, R.F., *The early history of x-ray diagnosis with emphasis on the contributions of physics 1895-1915.* Physics in Medicine & Biology, 1995. **40**(11): p. 1741-87.
3. Radon, J., *Uber die Bestimmung von Funktionen durch ihre integralwerte langs gewisser Mannigfaltigheiten.* Breichte Sachsische Akademie der Wissenschaften, 1917. **69**: p. 262-277.
4. Hounsfield, G.N., *Computerized transverse axial scanning (tomography): Part 1. Description of system.* The British Journal of Radiology, 1973. **46**(552): p. 1016-1022.
5. Kalender, W.A., *CT: the unexpected evolution of an imaging modality.* European Radiology Supplements, 2005. **15**(S4): p. d21-d24.
6. Townsend, D.W., T. Beyer, and T.M. Blodgett, *PET/CT scanners: a hardware approach to image fusion.* Seminars in Nuclear Medicine, 2003. **33**(3): p. 193-204.
7. BfS, *Jahresbericht 2017/2018*. 2018, Bundesamt für Strahlenschutz.
8. IOMP, *IOMP Policy Statement No 1 The Medical Physicist Role and Responsibilities*. 2012, International Organization for Medical Physics.
9. ACR, *2012 Computed Tomography Quality Control Manual*. 2012.
10. Strålsäkerhetsmyndigheten, *SSMFS 2018:5 Strålsäkerhetsmyndighetens föreskrifter om medicinska exponeringar*. 2018.
11. Nowik, P., et al., *Quality control of CT systems by automated monitoring of key performance indicators: a two-year study.* Journal of Applied Clinical Medical Physics, 2015. **16**(4): p. 254-265.
12. Merzan, D., et al., *Evaluating the impact of scan settings on automatic tube current modulation in CT using a novel phantom.* The British Journal of Radiology, 2017. **90**(1069): p. 20160308.
13. Nowik, P., et al., *The dosimetric impact of including the patient table in CT dose estimates.* Physics in Medicine & Biology, 2017. **62**(23): p. N538-N547.
14. Nowik, P., et al., *The synthetic localizer radiograph - A new CT scan planning method.* Physica Medica, 2019. **61**: p. 58-63.
15. Symons, R., et al., *Low-dose lung cancer screening with photon-counting CT: a feasibility study.* Physics in Medicine & Biology, 2017. **62**(1): p. 202-213.
16. Dangelmaier, J., et al., *Experimental feasibility of spectral photon-counting computed tomography with two contrast agents for the detection of endoleaks following endovascular aortic repair.* European Radiology, 2018. **28**(8): p. 3318-3325.
17. Aubrey, J., et al., *Measurement of skeletal muscle radiation attenuation and basis of its biological variation.* Acta Physiologica, 2014. **210**(3): p. 489-97.
18. ICRP, *ICRP Publication 103. The 2007 Recommendations of the International Commission on Radiological Protection.* Annals of the ICRP, 2007. **37**(2-4): p. 1-332.

19. Andersson, P., et al., *The radiation environment in Sweden*. 2007, Swedish Radiation Protection Authority.

20. Shope, T.B., R.M. Gagne, and G.C. Johnson, *A method for describing the doses delivered by transmission x-ray computed tomography.* Medical Physics, 1981. **8**(4): p. 488-95.

21. IEC, *61223-2-6 Evaluation and routine testing in medical imaging departments Part 26: Constancy tests Imaging performance of computed tomography X-ray equipment*. 2006, International Electrotechnical Commission.

22. McCollough, C., et al., *The measurement, reporting, and management of radiation dose in CT.* Report of AAPM Task Group, 2008. **23**(23): p. 1-28.

23. Andersson, J., et al., *Estimating Patient Organ Dose with Computed Tomography: A Review of Present Methodology and Required DICOM Information: A Joint Report of AAPM Task Group 246 and the European Federation of Organizations for Medical Physics (EFOMP)*. 2019.

24. DeMarco, J., et al., *A Monte Carlo based method to estimate radiation dose from multidetector CT (MDCT): cylindrical and anthropomorphic phantoms.* Physics in Medicine & Biology, 2005. **50**(17): p. 3989.

25. Caon, M., G. Bibbo, and J. Pattison, *An EGS4-ready tomographic computational model of a 14-year-old female torso for calculating organ doses from CT examinations.* Physics in Medicine & Biology, 1999. **44**(9): p. 2213.

26. Castellano, I., D. Dance, and P. Evans, *CT dosimetry: getting the best from the adult Cristy phantom.* Radiation Protection dosimetry, 2005. **114**(1-3): p. 321-325.

27. Gordon, R., R. Bender, and G.T. Herman, *Algebraic reconstruction techniques (ART) for three-dimensional electron microscopy and X-ray photography.* Journal of theoretical Biology, 1970. **29**(3): p. 471-481.

28. Beister, M., D. Kolditz, and W.A. Kalender, *Iterative reconstruction methods in X-ray CT.* Physica Medica: European Journal of Medical Physics, 2012. **28**(2): p. 94-108.

29. Ramirez-Giraldo, J., et al., *Radiation dose optimization technologies in multidetector computed tomography: a review.* Medical Physics International, 2014. **2**(2): p. 420-30.

30. Aggarwal, H.K., M.P. Mani, and M. Jacob, *MoDL: Model-based deep learning architecture for inverse problems.* IEEE transactions on medical imaging, 2018. **38**(2): p. 394-405.

31. Brooks, R.A. and G. Di Chiro, *Statistical limitations in x-ray reconstructive tomography.* Medical Physics, 1976. **3**(4): p. 237-240.

32. Nagel, H.D., *CT parameters that influence the radiation dose*, in *Radiation dose from adult and pediatric multidetector computed tomography*. 2007, Springer. p. 51-79.

33. Elojeimy, S., S. Tipnis, and W. Huda, *Relationship between radiographic techniques (kilovolt and milliampere-second) and CTDIvol.* Radiation Protection Dosimetry, 2010. **141**(1): p. 43-49.

34. Bushberg, J.T. and J.M. Boone, *The essential physics of medical imaging*. 2011: Lippincott Williams & Wilkins.

35. Gordic, S., et al., *Ultralow-dose chest computed tomography for pulmonary nodule detection: first performance evaluation of single energy scanning with spectral shaping.* Investigative Radiology, 2014. **49**(7): p. 465-473.

36. Strålsäkerhetsmyndigheten, *SSMFS 2008:31 Strålsäkerhetsmyndighetens föreskrifter om röntgendiagnostik*. 2009, Strålsäkerhetsmyndigheten.

37. Kuttner, S., et al., *A proposed protocol for acceptance and constancy control of computed tomography systems: A Nordic Association for Clinical Physics (NACP) work group report.* Acta Radiologica, 2012.

38. Zarb, F., L. Rainford, and M.F. McEntee, *Image quality assessment tools for optimization of CT images.* Radiography, 2010. **16**(2): p. 147-153.

39. Thilander-Klang, A., et al., *Evaluation of subjective assessment of the low-contrast visibility in constancy control of computed tomography.* Radiation Protection Dosimetry, 2010. **139**(1-3): p. 449-454.

40. ACR, *2017 Computed Tomography Quality Control Manual*. 2017.

41. IEC, *61223-2-6, Evaluation and routine testing in medical imaging departments – Part 2-6: Constancy tests – Imaging performance of computed tomography X-ray equipment.* 2006.

42. IEC, *61223-3-5, Evaluation and routine testing in medical imaging departments – Part 3-5: Acceptance tests – Imaging performance of computed tomography X-ray equipment.* 2004.

43. McCollough, C.H., M.R. Bruesewitz, and J.M. Kofler, Jr., *CT dose reduction and dose management tools: overview of available options.* Radiographics, 2006. **26**(2): p. 503-12.

44. Kalra, M.K., et al., *Techniques and applications of automatic tube current modulation for CT.* Radiology, 2004. **233**(3): p. 649-657.

45. Sookpeng, S., C.J. Martin, and D.J. Gentle, *Investigation of the influence of image reconstruction filter and scan parameters on operation of automatic tube current modulation systems for different CT scanners.* Radiation Protection dosimetry, 2015. **163**(4): p. 521-30.

46. Gudjonsdottir, J., B. Ween, and D.R. Olsen, *Optimal use of AEC in CT: a literature review.* Radiologic Technology, 2010. **81**(4): p. 309-17.

47. Tsalafoutas, I.A., et al., *Utilizing a simple CT dosimetry phantom for the comprehension of the operational characteristics of CT AEC systems.* Medical Physics, 2013. **40**(11): p. 111918.

48. Moro, L., et al., *Considerations on an automatic computed tomography tube current modulation system.* Radiation Protection dosimetry, 2013. **156**(4): p. 525-30.

49. Kanal, K.M., et al., *Impact of operator-selected image noise index and reconstruction slice thickness on patient radiation dose in 64-MDCT.* American Journal of Roentgenology, 2007. **189**(1): p. 219-25.

50. Muramatsu, Y., et al., *[Performance evaluation for CT-AEC(CT automatic exposure control)systems].* Nihon Hoshasen Gijutsu Gakkai Zasshi, 2007. **63**(5): p. 534-45.

51. Brisse, H.J., et al., *Automatic exposure control in multichannel CT with tube current modulation to achieve a constant level of image noise: experimental assessment on pediatric phantoms.* Medical Physics, 2007. **34**(7): p. 3018-33.

52. Goo, H.W. and D.S. Suh, *The influences of tube voltage and scan direction on combined tube current modulation: a phantom study.* Pediatric Radiology, 2006. **36**(8): p. 833-40.

53. Papadakis, A.E., K. Perisinakis, and J. Damilakis, *Automatic exposure control in pediatric and adult multidetector CT examinations: a phantom study on dose reduction and image quality.* Medical Physics, 2008. **35**(10): p. 4567-76.

54. MHRA, *CT scanner automatic exposure control systems*. 2005: MHRA Report 05016.

55. Sookpeng, S., C.J. Martin, and D.J. Gentle, *Comparison of different phantom designs for CT scanner automatic tube current modulation system tests.* Journal of Radiological Protection, 2013. **33**(4): p. 735-61.

56. Wilson, J.M., et al., *A methodology for image quality evaluation of advanced CT systems.* Medical Physics, 2013. **40**(3): p. 031908.

57. Habibzadeh, M.A., et al., *Impact of miscentering on patient dose and image noise in x-ray CT imaging: phantom and clinical studies.* Physica Medica, 2012. **28**(3): p. 191-9.

58. Szczykutowicz, T.P., A. DuPlissis, and P.J. Pickhardt, *Variation in CT Number and Image Noise Uniformity According to Patient Positioning in MDCT.* American Journal of Roentgenology, 2017. **208**(5): p. 1064-1072.

59. IAEA, T., *457. Dosimetry in Diagnostic Radiology: An International Code of Practice*. 2007, Technical Reports Series, Vienna: IAEA.

60. Jones, D.G. and P.C. Shrimpton, *Survey of CT practice in the UK. Part 3: Normalised organ doses calculated using Monte Carlo techniques*, in *National Radiological Protection Board publication, NRPB-R250*. 1991, National Radiological Protection Board.

61. Schmidt, B., et al., *Assessment of patient dose from CT localizer radiographs.* Medical Physics, 2013. **40**(8): p. 084301.

62. ICRP, *ICRP Publication 110. Realistic reference phantoms: an ICRP/ICRU joint effort. A report of adult reference computational phantoms.* Annals of the ICRP, 2009. **39**(2): p. 1-164.

63. Petoussi-Henss, N., et al., *The GSF family of voxel phantoms.* Physics in Medicine & Biology, 2002. **47**(1): p. 89-106.

64. Kalender, W.A., *Dose in x-ray computed tomography.* Physics in Medicine & Biology, 2014. **59**(3): p. R129-50.

65. Geisler, E. and O. Heller, *Management of medical technology: theory, practice and cases*. Vol. 2. 2012: Springer Science & Business Media.

66. Yin, Z., et al., *Acquisition, preprocessing, and reconstruction of ultralow dose volumetric CT scout for organ-based CT scan planning.* Medical Physics, 2015. **42**(5): p. 2730-9.

67. Gomes, J., et al., *An Investigation of Low-Dose 3D Scout Scans for Computed Tomography.* Proceedings of SPIE--the International Society for Optical Engineering, 2017. **10132**.

68. Norman, G., *Likert scales, levels of measurement and the "laws" of statistics.* Advances in Health Sciences Education, 2010. **15**(5): p. 625-32.

69. Sullivan, G.M. and A.R. Artino, Jr., *Analyzing and interpreting data from likert-type scales.* Journal of Graduate Medical Education, 2013. **5**(4): p. 541-2.

70. McMillan, K., et al., *MO-E-17A-01: BEST IN PHYSICS (IMAGING)–Calculating SSDE From CT Exams Using Size Data Available in the DICOM Header of CT Localizer Radiographs.* Medical Physics, 2014. **41**(6): p. 423-424.

71. McCollough, C., et al., *Use of water equivalent diameter for calculating patient size and size-specific dose estimates (SSDE) in CT: the Report of AAPM Task Group 220.* AAPM report, 2014. **2014**: p. 6.

72. Heiken, J.P., et al., *Dynamic incremental CT: effect of volume and concentration of contrast material and patient weight on hepatic enhancement.* Radiology, 1995. **195**(2): p. 353-7.

73. Bae, K.T., *Intravenous contrast medium administration and scan timing at CT: considerations and approaches.* Radiology, 2010. **256**(1): p. 32-61.

74. Svensson, A., et al., *Hepatic contrast medium enhancement at computed tomography and its correlation with various body size measures.* Acta Radiologica, 2012. **53**(6): p. 601-6.

75. Yamashita, Y., et al., *Abdominal helical CT: evaluation of optimal doses of intravenous contrast material--a prospective randomized study.* Radiology, 2000. **216**(3): p. 718-23.

76. Han, J.K., et al., *Contrast media in abdominal computed tomography: optimization of delivery methods.* Korean Journal of Radiology, 2001. **2**(1): p. 28-36.

77. Yanaga, Y., et al., *Effect of contrast injection protocols with dose adjusted to the estimated lean patient body weight on aortic enhancement at CT angiography.* American Journal of Roentgenology, 2009. **192**(4): p. 1071-8.

78. Zhang, Q., M.J. Guo, and Y.F. Wu, *Correlation of abdominal fat ratio with hepatic CT enhancement.* Experimental and Therapeutic Medicine, 2015. **10**(1): p. 285-288.

79. Akaike, H., *Information Theory and an Extension of the Maximum Likelihood Principle,* in *Selected Papers of Hirotugu Akaike*. 1998, Springer. p. 199-213.

80. Hurvich, C.M. and C.L. Tsai, *Regression and Time-Series Model Selection in Small Samples.* Biometrika, 1989. **76**(2): p. 297-307.

81. Wagenmakers, E.J. and S. Farrell, *AIC model selection using Akaike weights.* Psychonomic Bulletin & Review, 2004. **11**(1): p. 192-196.